Numerical process studies of the impact of mesoscale dynamics on primary production in the Arctic Marginal Ice Zone

NERSC Technical report no. 219
August 2002

Kjetil Lygre, Ola M. Johannessen and Helge Drange
Nansen Environmental and Remote Sensing Center, Bergen, Norway

Short title: EDDIES AND PRIMARY PRODUCTION IN MIZ

Abstract. The effect of mesoscale eddies on the primary production in the Arctic MIZ is investigated numerically by using a dynamical model utilizing an isopycnic layer formulation coupled to an ice model and a 5 compartment NPZD ecosystem model.

Idealized experiments are carried out to investigate the response of the ice-ocean system and the ecosystem for various wind scenarios acting on an ice edge. A novel feature is the employment of a simple parameterization making the wind stress dependent on the ice state yielding typically maximum stress on the ocean surface for intermediate ice concentrations. The only specification is the wind vector on top of the atmospheric boundary layer.

The results agree with classical theory in that up-welling ocurs near the ice edge when a wind is blowing with the ice to the right – ITR – (in the northern hemisphere). Growth is increased both due to light abundance and entrainment of nutrient from below. A more pronounced additional effect is the formation of an ice-edge jet which whithin a few days disintegrates into eddies. The energy transfer feeding the process is relatively modest, because the ice edge is compacted and the region of maximum stress is narrowed. The resulting weak cyclones (O(5km)) are very effective in transporting nutrient from the ice covered to the open water, enhancing biological growth within a 5 kilometers wide band along the ice edge several days after the initial burst.

In the ITL case (opposite wind) the wind expands the MIZ, widening the region with high stress, such that energy is comparably more efficiently transferred to the ocean. Eddies are anticyclonic, larger (15 km) and more energetic. Biological growth is enhanced over a 20 km wide stripe, while some inhibition due to shading of ice bands extending off-ice takes place. In an experiment examining the effect of a wind turning 360 degrees (ITR-ITL-ITR), the resulting response yielded a qualitatively similar pattern as the ITR case, but with a stronger response due to the energizing during the ITL period.

A common qualitative feature for all cases, independent of wind history, is the petsistence of eddies along the ice edge transporting nutrient from the unaffected ice-covered portion, to the open water which is void of nutrient. As such it behaves as a horizontal analogue of the deep chlorophyll maximum in the vertical. The small scales involved imply that there may be large sampling errors for the biogeochemical fields in reality.

Introduction

The physical and biological processes in the Arctic Ocean are driven by atmospheric radiation and high latitude circulation of air and ocean water masses. The location of the marginal ice zone (MIZ), which has large seasonal and interannual variability in the Barents Sea area, is dependent on several large scale physical processes such as inflow of Atlantic water, outflow of sea ice and polar water from the Arctic ocean, and the prevailing atmospheric conditions. The biological processes are mainly governed by the ice edge location, chemical composition of the water, light and radiation conditions and physical processes such as mixing, stratification and circulation of the water masses. The current view is that meltwater supplied from the retreating ice-edge stabilizes the water coloumn and reduces vertical mixing, while the modest ocean depth limits wind-induced dispersion of phytoplankton. A wind episode can promote biological growth by entraining nutrient rich waters from below, while at the same time slowing growth by mixing down phytoplankton, which becomes light-inhibited. The net effect is that winds of episodic nature tend to be be optimal for growt.

The first detailed investigations of the MIZ were made north of Svalbard in 1977, where upwelling during strong wind events was found to be an important mechanism to bring deeper water masses towards the surface [Buckley *et al.*, 1979]. During proceeding more extensive experiments, processes such as upwelling (downwelling) with associated divergence (convergence) at the surface, ice edge jets, ice edge meanders and eddy formation and advection were studied (NORSEX-79, Johannessen et al., 1983). During the Marginal Ice Zone experiments from 1983 to 1987, a number of physical and biological investigations were carried out in the Fram Strait, Greenland Sea and Barents Sea (e.g. [Johannessen *et al.*, 1987]) The Seasonal Ice Zone Experiments (SIZEX) in the Barents Sea in 1989 and 1992, several focused on ice edge variability, current and water mass structures, impact of wind forcing, tides and bottom topography ([Sandven *et al.*, 1991]; [Sandven and Johannessen, 1993]).

During the last decade it has become clear that processes taking place on a variety of space and time scales have large impact on primary production. For instance, [Eilertsen and Wyatt, 2000] and others have found that the most important controls on growth are light (ice/non-ice), concentration of bottom trapped resting spores, and turbulent mixing energy. Thus, the open water areas can be as important as the MIZ in initiating the blooms. [Falk-Petersen *et al.*, 2000] did not find any signs of a bloom folowing the retreating ice edge during two years, but emphasized interannual variability of the ice cover and the regional ocean-atmosphere patterns as a dominant driving force. Also cooling episodes have been suggested as a trigger for bloom initiation, as convection can extend to the bottom during destabilisation of the water column an thus mixing in diatom spores from the bottom sediments, a process dubbed as *phyto-convection* by [Backhaus *et al.*, 1999].

It is of great importance to understand the controling physical mechanisms on primary production, as marine ecosystems are responsible for about 50% of our planet's plant - biomass production. While southern temperate and Antarctic systems are relatively well understood, this is not so for the Arctic regions. While both botanical and zoological aspects of open water ecology relative to hydrography have been relatively thoroughly studied ([Båmstedt *et al.*,

1991] [Eilertsen *et al.*, 1989] and refs. therein), the literature dealing with ice edge systems is rather scarce and purely deals with limited biological aspects, although the multidisciplinary studies of [Falk-Petersen *et al.*, 2000] strongly links the interannual variability of the ice cover to the annual production, among other things.

Due to the favoral factors of the Arctic shelves, the primary production can reach 400–2000 [1] mmolN $m^{-2}y^{-1}$there, the Bering Sea being the most productive region. In the Barents Sea the densest algae stocks are typically 4–7.6 mmolN m^{-3}, while the maximum primary productivity and production are found to be 2.5 mmolN $m^{-3}d^{-1}$and 19 mmolN $m^{-2}d^{-1}$, respectively [Sakshaug *et al.*, 1992]. Also the permanently ice-covered Arctic may have primary production as high as 250 mmolN $m^{-2}y^{-1}$ [Pomeroy, 1997], despite the light limiting conditions.

A marked dynamical influence of a MIZ is the way it can modify the resulting stress on the ocean. By typically blowing along the ice-edge with the ice pack to the right[2] (ITR, hereafter) and if the ice is drifting, the wind will imply a larger stress on the ocean over the MIZ than over the open ocean ([Buckley *et al.*, 1979]; [Johannessen *et al.*, 1983]; [Häkkinen, 1986]; but note important modifications in [Fennel and Johannessen, 1998]). A divergent iceward Ekman transport is induced, resulting in an upwelling with a maximum amplitude at the ice edge and decaying with the deformation radius R_d at the sides [Fennel and Johannessen, 1998]. Nutrients (and other properties) from beneath the mixed-layer (ML) are thus brought into the euphotic zone, and may be subject to increased mixing etc. The ocean adjusts geostrophically to the elevated isopycnals, implying an along-wind jet inside the MIZ and a countercurrent in the open ocean. The mechanism is also held as one of several explanations for deep-water formation [Häkkinen, 1987b].

The opposite case with the wind blowing with the ice to the left (ITL, hereafter) can occur episodically, e.g. due to atmospheric synoptic variability, or may prevail during the summer half year. Accordingly, the ocean responds by forming an ITL ice-edge, water downwells at the ice-edge and plankton growth is inhibited because of light extinction. However, additional factors such as the state of the ice, thermodynamic effects, along-edge variability, dynamic instability, the properties of the atmospheric boundary layer complicate the picture ([Johannessen *et al.*, 1983]; [Guest *et al.*, 1995]; [Fennel and Johannessen, 1998]). Furthermore, in the case the ice is not moving, the ocean response will be opposite to the case where the ice is in motion. A detailed discussion of these issues are given in the modelling section.

Another prominent characteristic of the MIZ is the presence of mesoscale eddies which may be caused by instabilities of the ice-edge jet or of an already existing current. Their diameter typically scale with the first internal radius of deformation, R_d (here a few kilometers). Studies in the East Greenland Current also suggest topographic influences as

[1] All biomass measures are given as mmolN. All referred numbers given in gC from the literature are converted according to the formula 1 gC = 12.6 mmolN, and rounded to two digits. A ratio C:N=106:16 is prescribed.

[2] in the northern hemisphere

dominating ([Johannessen *et al.*, 1983]; [Johannessen *et al.*, 1987]; [Häkkinen, 1987a]). Cyclonic (anticyclonic) eddies imply a doming (deepening) of the pycnocline and have an effect on the biogeochemical system, in analogy with the up(down-)welling cases described above. [Niebauer and Smith, 1989] demonstrated, by simply imposing eddy structures on a pre-existing MIZ in a 2-D (xz) model, the effectiveness of a cyclone in diverting the ice pack and triggering phytoplankton growth. A similar effect was noted at the rims of an anticyclone. The experiment demonstrated that the response of the ecosystem is not necessarily linear with respect to the physical conditions. Here it should also be noted that the Fram Strait is an exceptional part of the MIZ, in that its depth typically exceeds 2000 m [Smith, 1987]. Hence, the seasonal shift of the ice-edge is comparably small, and the impact of ice-edge processes (up-welling events, eddies) are present throughout the year and are relatively more influential than for the shallow seas.

Quantifications of the influence of mesoscale dynamics on the MIZ ecosystem ar few or non-existent, due to the prohibitive logistic bearings. For the Bering Sea continental shelf [Smith, 1987] estimated that the ice-edge system accounts for 40% of the annual primary production. [Manley and Smith, 1994] suggested that instabilities of the Northern Greenland Sea rim in combination with cooling woul create narrow cyclones in which biogenic material would sink along isopycnal surfaces. From other eddy rich areas like the Kuroshio frontal region [Kimura *et al.*, 1997] estimated the carbon production due to eddies to 490 mmolN $m^{-2}y^{-1}$, a significant part of the total and consistent with similar studies from the Gulf Stream. The pumping of nutrients due to planetary waves has been stydied by e.g. [McGillicuddy *et al.*, 1999], and the global effects have been estimated by [Uz *et al.*, 2001]. However, the eddies of the Arctic tend to be relatively narrow and short lived, so a generalization from other regions cannot be made.

Due to its turbulent nature, mesoscale dynamics is especilly tractable by numerical modelling. [Smith *et al.*, 1996] simulated wind-foced open ocean processes in the North Atlantic using a simple coupled physical-ecosystem model and found a stronger spatial variability of the ecosystem than that of the dynamical fields. The over-all effect of eddies on production was not significant, although the relative role of new vs. regenerate production increased notably. Increase in new production with spatial resolution was also found by [Mahadevan and Archer, 2000] who used a non-hydrostatic model. The effect was most notable for up-welling and nutrient uptake, rather than e.g. temperature. Nutrient supply ocured primarily where isopycnals outcropped at the base of the euphotic zone.

Recently, [Spall and Richards, 2000] used a fully coupled physics-ecosystem model based on isopycnic layers in investigating the effects of frontal dynamics. The frontal instabilities imply both increased upwelling of nutrients as well as subduction of phytoplankton. Typical increases in primary production amount to 100 % locally and 10 % over the total frontal region, indicating a significant contribution to the strength of the biological pump. [Martin *et al.*, 2001] ecxtended the study by allowing small and large phyto- and zoo plamkton, showing that the various size classes exist in various dynamical regimes.

Motivation of the present study

In order to advance our knowledge on the above issues a project "Ecological studies in the Marginal Ice Zone and response to physical forcing" was carried out during 1996—1999, both covering field studies and modelling experiments, focusing on mesoscale ice edge dynamics, including ecosystem dynamics.
It is for the first time that such a focused and interdiciplinary project has been carried out in the Arctic MIZ. The focus of our paper is a bit more specialized, dealing with the non-linear response of the MIZ to various wind situations simulated numerically, including the response of the low-trophic ecosystem to the resulting mesoscale features. The latter imply, for instance, strong heterogenity of light availability due to shading by the ice. Besides the ecosystem response, we also aim at shedding light over the relevance of previous idealized experiments by introducing a lowest order parametrization of the wind stress which makes no a priori assumptions about the cross-edge stress profile or whether ice is moving or fast. The questions we attemt to answer are:

What is the dynamical response of the ocean-ice system to different wind episodes?
What are the effects on the ecosystem of such forcing?
What are the integral implications on primary production?

The initial conditions and identification of scales have been derived from the collected hydrographic and remote sensing data, of which the most relevant will be presented in the following. Second, the model is presented, followed by - third - a section describing the experiments. Fourth, the results are discussed and finally, the paper is concluded.

Data

During the project period two cruises with R/V *Håkon Mosby* were carried out in the Fram Strait region under NERSC's conduct, one in Aug 1996 and one in May 1997. Here only data from the former will be shown, since they are more detailed and sufficiently illustrative for motivating the model experiments. The aim of the field campaigns was not to track the effect of certain wind episodes, so here we only describe the relevant data sets. In the following it is focused on the time window around Aug 10, when the ship profiled W–E approximately along the ice edge.

Sea-ice and meteorological conditions: From SAR imagery ice features derived from the ERS-1 SAR on Aug 9 show a sharp ice edge aligned approximately W–E along 80 °40' N. The sharpness is most likely due to the sustained action of the wind, packing the ice together. S-SW winds of typically 10–15 ms^{-1} prevailed throughout Aug 9, while calming on Aug 10. [Furevik and nd A. D. Sandvik, 2002] validated and discussed wind measurements from the ship and derived from SAR and from a model for this location. Predictions with a simple model hold that modest iceward motion shall ocur when the wind is blowing at right angle towards the ice [Ikeda, 1989].

Weak wave signatures are evident on the sharp ice edge; in the very western portion (9–11 °W) waves of approx. 20 km long-edge and 4 km cross-edge are clearly detectable. Further eastwards there is more irregular variability. The correspondence in scale of these features with the hydrography shown in the following, is intriguing , alhtough no clear link can be drawn between the two phenomena from the present data set. It should also be mentioned that the ship track crosses in and out of the coastally trapped branch of the strong barotropic West Spitsbergen Current [Fahrbach *et al.*, 2001], implying significant dynamical and thermodynamical constraints on th eice edge location. Around 16 °E the ship had to circumvent an ice tongue which had developed from th eice edge and was not visible on Aug 9. On Aug 10 it has been advected towards NE, implying a translation speed of about 0.4 ms^{-1}.

After Aug 10 the wind is relaxed to less than 5 ms^{-1} without any defined direction. The images from Aug 13 and 14 now showxs eddy or filament structures with a characteristic scale of 10 km [Furevik and nd A. D. Sandvik, 2002]. We conclude at this stage that during strong, steady, winds with a dominant on-ice component prevailing for 2 days or more the ice edge is compacted - even sharpened like a step function -, whereas during weak winds the ice and ocean display much more energetic features, although the invisibility of ocean structures during strong winds is a more plausible explanation. Whether this energetic state is a direct consequence of the preceeding wind episode will be of focus in the following.

Hydrography:

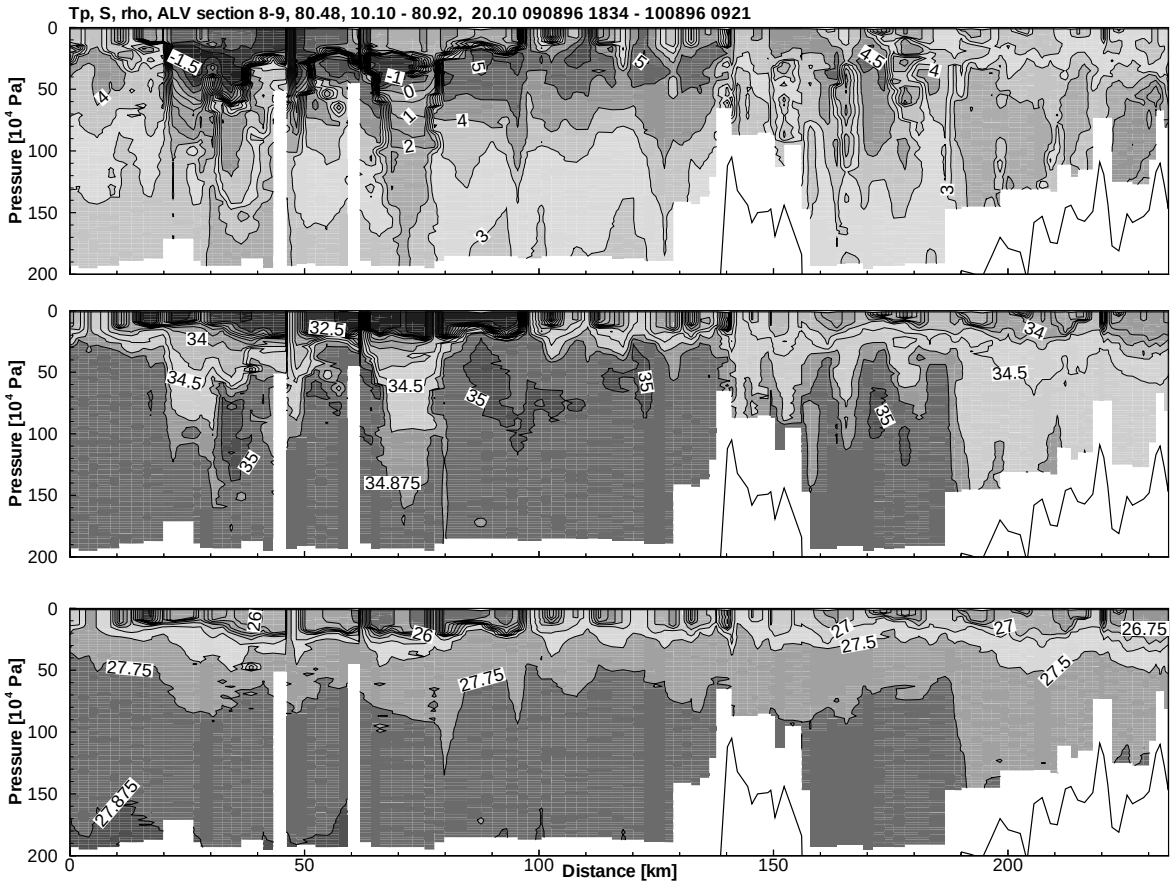

Figure 1. Towed CTD section taken north of Svalbard along the ice-edge W to E on 9–10 Aug 1996The leg between about 130 and 160 km deviates from the persistent eastward course by making asouthward loop (out of the paper plane).

A representative hydographic section of the area is shown in Fig. 1 in which the signature of the Atlantic layer is clearly seen typically below 25 m depth (core properties $T = 5^\circ$ C, $S = 35.0$). The main body is located between km 80 and 140, corresponding to the eastward principal branch of inflow to the Arctic. Further east, the slightly colder and fresher water type indicates mixing with the West Spitsbergen Current and coastal waters. The abrupt topography in this portion and the generally complicated bathymetry of the area imply strong topographic steering of the flow and local recirculations. Thus care must be taken in flux and volumetric calculations.

The main pycnocline is located at typically 20 m, sometimes shoaling to near surface (< 10 m), i.e. outside the profiling interval. Horizontal temperature and salinity gradients are as large as $0.5 \times 10^{-3\circ}$ Cm^{-1} and $0.4 \times 10^{-4}\mathrm{m}^{-1}$, respectively.

The second principal source water mass is the Polar Water to the west of km 100, comprising the upper 25 metres ($T \leq 0^\circ$ C, $S \leq 34.1$). This water mass can mix isopycnally with the upper part of the Atlantic Water. Indeed, that such mixing is taking part is clearly evident from the plentiful ocurrences of intrusive layering, most clearly seen at km 20–35, 65–80, and also in the eastern portion, which is more influenced by coastal waters, km 160–190. The notoriously complicated interplay with such intrusions and other characteristics of the flow is far beyond the scope of this paper; the reader should refer to [Kuzmina, 2000] and [May and Kelley, 1997] for recent discussions. We only emphasize that under certain regimes, intrusions can be driven by baroclinic instability, a well-known mechanism of the Arctic frontal system ([Johannessen *et al.*, 1983]; [Johannessen *et al.*, 1987]). *A priori* one could thus hypothesize that the horizontal scales emanent from intrusions are the same as that of an underlying mechanism. This scale is roughly 25 km from Fig. 1, a number that is confirmed from other sections (not shown). A full discussion of the hydrographic measurements will be reported elsewhere.

Modelling approach

The model concept we have chosen is the coupled ocean-ice-biogeochemical system by [Drange, 1997], with some recent modifications described in the following. The model is based on an isopycnic layer formulation, which is especially tractable when studying phenomena broadly governed by potential vorticity dynamics (eddies, subduction). [Spall and Richards, 2000] have successfully demonstrated a practically similar model system applied for a sub-mesoscale study.

The authors have long experience with the model applied to large scale phenomena Here it is set up for a periodic channel 50 km long and 100 km wide (the latter dimension in order to minimize boundary effects). One half of the channel is ice covered initially and the ice/ocean is forced by spatially uniform (except at the boundaries) but time-dependent wind. Details on the model features, initial conditions and forcing are given below.

Special features of the physical model

Wind and ice-to-ocean stresses: Many investigators have tacled the atmosphere-ice-ocean momentum transfer problem simply by essentially assuming a free-drift ice with some specification of constant drag coefficients for the three stresses between the respective interfaces (e.g. [Häkkinen, 1986]; [Johannessen *et al.*, 1994]). Doing so one is limited in interpretation by the inherent assumption. In reality one is dealing with a system with strong interactions between all sub-systems (ocean-atmosphere-ice). The net effects of these have strong impact on the biogeochemical system, which in turn may feed back by the phytoplankton-light absorption-heating-stability link.
In order to advance our knowledge, we have started modestly by introducing a simple assumption of a wind stress which is a function of the ice/ocean state, in order to capture the lowest order effects.

[Fennel and Johannessen, 1998] reviewed the various assumptions on the cross ice-edge stress profiles and determined the oceanic response analytically. In brief, there are two classes of situations: One in which the MIZ is moving and a response similar to the one described in the introduction occurs (ice-edge upwelling). If the ice is non-moving, however, as in a case in which the MIZ has been compacted due to winds prevailing for several days, the response will be symmetrically opposite (because the stress on the ocean is discontinually *reduced* to nil at the ice-edge when viewed from the open ocean; i.e. identical to the ITL case with moving ice). For the moving ice ITR case, another robust result was that the importantmost feature of the stress profile is the strength of the stress step at or near the ice-edge, the structure inside the ice having a minor role. Similarly, the along-ice down-wind jet in the MIZ is also a robust feature, whereas the counter-current is dependent on stress profile. The latter is rather of theoretical interest, as a barotropic current will probably in reality compensate the effect of the counter-current, the *horizontal shear* being unaffected. The study did not take account of processes such as thermodynamics, dynamical instability of the ice-edge jet, or realistic cross-edge movement of the ice. The latter two are the focus of the present study.

In searching for a new and useful stess formulation, we have (in accord with [Fennel and Johannessen, 1998]) been guided by the findings by [Guest *et al.*, 1995], who measured the surface roughness and the characteristics of the atmospheric boundary layer (ABL) and derived cross-edge stress profiles. In the following we refer primarily to a typical early spring situation with cold air outbrakes over the ocean with air flow from the Polar region, implying a cold stable air mass over the ice.

Briefly stated, the wind stress magnitude is (1) *decreasing* with increasing stability of the ABL and (2) *increasing* with the roughness of the underlying surface, when assuming some geostrophic wind speed at height. The exact magnitude of the wind speed and its reference level is irrelevant at our present level of idealization (as argued in [Guest *et al.*, 1995]). The stability is parameterized by h_A, the height of the ABL, increasing with decreasing stabilty, and assumed homogenous in the along-edge direction. In addition, the stress vector is deflected down-pressure-gradient relative to the wind direction. The angle of deflection is increasing

both with stability and roughness. The roughness parameter c_d is assumed to be a function only of the ice concentration, q.
Typically h_A is small inside the compact ice, increasing over the MIZ, being large over the ocean. c_d is taken to be moderate over the compact inner ice, high inside the MIZ, and relatively low over the ocean. The net effect of these two competing effects is a stress maximum just inside the ice-edge, as it "should". The actual stress to the ocean is of course depending on the ice motion, or lack thereof.

Accordingly, denoting the cross-(along)edge co-ordinate by $x(y)$, with x positive and large for the open ocean, we specify h_A as a piecewise linear function of x and $x_0(t)$, where x_0 is the time dependent average location of the ice-edge. c_d is taken as a piecewise linear function of $q = q(x, y, t)$. At every time step q is averaged over y, while putting $y = \max(y, 0.25)$, yielding $\bar{q}(x, t))$, and $x_0(t)$ is found implicitly from

$$\bar{q}(x_0) = 0.35 \tag{1}$$

The constants involved here have been determined from som preliminar experimentation, but are not sensitive parameters. The algorithm was developed with the aim to relate the ABL parameters to the ice edge. As the latter can move cross-ice, the ABL must follow it with the exception that the atmospheric scales are much larger than the oceanic ones, hence the smoothing of q. The relationship between q and h_A thus implies a back-coupling from the ocean to the atmosphere. So, by definition, the model system has a fully interacting — although crudely parameterized — atmosphere. Accordingly:

$$|\vec{\tau_a}| = r \times |\vec{W}| \tag{2}$$

$$r = \left[\left([C_1 \cdot f_d]^2 + \frac{1}{4} \right)^{\frac{1}{2}} + \frac{1}{2} \right]^{-1} \tag{3}$$

$$\theta = \arctan \left[\left(\left[(C_2 \cdot f_d)^2 + \frac{1}{4} \right]^{\frac{1}{2}} - \frac{1}{2} \right)^{\frac{1}{2}} \right] \tag{4}$$

$$f_d = \frac{c_d W}{f h_A} \tag{5}$$

$$c_d = \begin{cases} c_{dq} & \text{for } q > 0.9 \\ (c_{dq} - c_{dm}) \cdot \frac{(q-0.35)}{0.55} + c_{dm} & \text{for } 0.9 \geq q > 0.35 \\ (c_{dm} - c_{do}) \cdot \frac{(q-0.01)}{0.34} + c_{do} & \text{for } 0.35 \geq q > 0.01 \\ c_{do} & \text{for } 0.01 \geq q \end{cases} \tag{6}$$

$$h_A = \begin{cases} 250 & \text{for } x - x_0 < 10 \\ 600 + 35 \cdot (x - x_0) & \text{for } -10 \leq x - x_0 < 10 \\ 950 & \text{for } 10 \leq x - x_0 \end{cases} \tag{7}$$

$$\tag{8}$$

in which h_A is in meters and x in kilometers, $\vec{w}$ is the geostrophic wind vector with magnitude W, r the reduction factor, θ the turning angle, f the Coriolis parameter taken at 80° N. ρ_a and

ρ are the air and sea-water densities. For numerical purposes, i.e. due to the typically narrow realized MIZ, we had to put $c'_{dm} = 10 \cdot c_{dm}$ and then $c_d = \min(c_d, c_{dm})$, in order for the MIZ to experience a stress maximum at all. The two empirical constants $C_1 = 2.5$ and $C_2 = 0.5$ are selected as in the main reference, but in a realisting setting, they should be considered as tuning parameters.

The ice-to-ocean $\vec{\tau_i}$ and ocean $\vec{\tau}$ stresses are given by:

$$\vec{\tau_i} = \frac{\rho_i}{\rho}(\vec{u_i} - \vec{u}) \cdot |\vec{u_i} - \vec{u}| \quad (9)$$

$$\vec{\tau} = \vec{\tau_a} \cdot (1 - q) + \vec{\tau_i} \cdot q \quad (10)$$

and the involved constants are provided in Table .

Table 1. Constants in the stress formulation

f	$1.4 \cdot 10^{-4}$ s^{-1}
ρ_a	1.0 kgm^{-3}
ρ_i	900 kgm^{-3}
c_{do}	$0.8 \cdot 10^{-3}$
c_{dq}	$2.2 \cdot 10^{-3}$
c_{dm}	$5.0 \cdot 10^{-3}$

In summary, we have now to our disposal a stress formulation applicable to a wide type of situations (e.g. ice state shifting from free drift to compact ice in the same scenario) and capturing important features of atmosphere-ice-ocean interaction. Initial validation of the model run in 2-D mode (the xz-plane), showing a general agreement with the analytical solutions is provided in the appendix.

Upwelling, wind-generated entrainment, TKE and u_*: While authors like [Häkkinen, 1986] have focused on investigations of upwelling near an ice-edge for various along edge disturbances, they tended to neglect the entrainment arising from the direct wind-mixing. The entrainment is mainly governed by the cube of the friction velocity, $u_* = \sqrt{\tau/\rho} = \sqrt{c_d \rho_a / \rho} U_w$. For a wind acting over some time (a few days) the deepening of the ML can be substantial. The entrainment is enhanced where the pycnocline shoales (inside cyclonic features) since less mixing energy is needed. For the ecosystem this mechanism is fundamental in bringing nutrients into the ML.

Sea-ice: While the modelling of ice mechanics is under development and still a challenge to ice-modellers as the spatial scales are becoming comparable to the floe dimension, we were forced to take the well-known state-of-art approach deriving from the early work of [Hibler, 1979], assuming the ice is a 2-D continuum and applying a viscous-plastic rheology. We deem this approach sufficient for our purpose, given the substantial lack of observations of parameters relevant to ice mechanics. We choose a low value for the ice strength P^*=2000Nm^{-2} to make

the ice easily deformable (Markus Harder, personal communication), as should be expected in the MIZ.

Thermodynamic ice-ocean coupling: Whenever timescales are smaller than O(1 day) and spatial scales are below O(10 km) – both conditions apply here –, one cannot take the familiar approximation that ice melts instantaneously, i.e. during a model time step, when exposed to ocean temperatures above freezing point. Since, in addition, we will apply a – in this regard – low vertical resolution, we rather use the empirical relationship according to [Josberger, 1987]

$$\frac{\partial(T - T_f)}{\partial t} = c_g \cdot u_* \cdot \frac{(T_f - T))}{h_{ML}} \tag{11}$$

in which h_{ML} is the ocean ML thickness, T temperature, T_f freezing point of seawater, u_* is the friction velocity and $c_g = 8.1 \times 10^{-3}$ is an empirical constant. (The not exact equality with [Josberger, 1987] is because here we use u_* while he used $|\vec{u_i} - \vec{u}|$.) Typically the temperature deviation from freezing below the ice is several tenths of a degree at the ice edge, decaying to nil whithin 10–20 km.

Moreover, the low vertical resolution (h_{ML} = O(10 m)) combined with the extremely small model time step ($\Delta t = 8$ s), imply an inconsistency between the bulk parameterizations of the surface heatfluxes and the small spatiotemporal scales experienced with the current lay-out. For instance, to translate to ice thickness changes from Eq. 11 one applies the relation

$$\frac{\partial h_i}{\partial t} = -\frac{c_p \rho h}{L \rho_i} \frac{\partial(T - T_f)}{\partial t} \tag{12}$$

i.e., an equivalent amount of heat corresponding to the temperature change times a layer thickness is used to melt ice during a time step. However, it is obvious that a ML of several tens of meters cannot experience such a change within such a small timestep. Therefore, we crudely account for this process by assuming that any disturbance from the surface has a finite and constant downward propagation velocity $w_{con} = 0.1\text{ms}^{-1}$ implying an effective ML thickness $h_{con} = w_{con}\Delta t = 0.8$ m. Henceforth, we put $h = h_{con}$ when computing all surface fluxes, and taking

$$f(t + \Delta t) = f(t) \cdot \left(1 - \frac{h_{con}}{h_{ML}}\right) + f^*(t + \Delta t) \cdot \frac{h_{con}}{h_{ML}} \tag{13}$$

where f is T or S and f^* is the provisional values based on h_{con} alone. The resulting ice-ocean coupling acts as a time-filter and is in effect consistent with formulations applied in resolved experiments, e.g. [Kämpf and Backhaus, 1998]. The neglect of this modification would typically overestimate ice melt rate by a factor 10, implying a corresponding change in the buoyancy flux, with spurious feed-back to h.

The model equations

The model system the coupled physical-biogeochemical model by [Drange, 1997] with the ecosystem (in nitrogen quantities) model by [Broström, 1997]

Physical and ice modules. The equations that are solved are the momentum equation:

$$\frac{\partial \vec{u}}{\partial t} + \nabla \frac{\vec{u}^2}{2} + (\zeta + f)\vec{k} \times \vec{u} + \nabla M = \frac{1}{\Delta p} \nabla \cdot (\nu \Delta p \nabla \vec{u}) \tag{14}$$

and the continuity equation:

$$\frac{\partial \Delta p}{\partial t} + \nabla \cdot (\vec{u} \Delta p) = \frac{1}{\Delta p} \nabla \cdot (A_p \Delta p \nabla \vec{u}) \tag{15}$$

where $\vec{u} = (u, v)$ is the horizontal vector, ζ is the vertical component of the relative vorticity, $M = gz + p\alpha$ is the Montgomery potential with α specific volume, Δp is layer thickness, p pressure, g gravity, f is the Coriolis parameter, ν is the eddy viscocity set equal to 1 $\mathrm{m^2 s^{-1}}$, and A_p is layer thickness diffusion set equal to 0.5 $\mathrm{m^2 s^{-1}}$.

For temperature and salinity in the mixed layer and temperature in the interior layers we have:

$$\frac{\partial \Delta p\, a}{\partial t} + \vec{u} \cdot \nabla (\Delta p\, a) = \nabla \cdot (A_h \Delta p \nabla a) + w_{interface} \frac{\partial a}{\partial p} + F(a, z) \tag{16}$$

for $a = (S, \theta)$ salinity or potential temperature. A_h is horizontal (or isopycnal) diffudsivity, set equal to 1 $\mathrm{m^2 s^{-1}} = \nu$, F is the forcing, which is zero in the interior and finite only at the surface. $w_{interface} \frac{\partial a}{\partial p}$ denotes the diapycnal mixing which – except for the ML base – is proportional to the stability and chosen such as to maintain potential density. In these experiments this term is negligible. For interior salinity the equation of state is solved for S from θ and σ.

For the ice thickness[3] h_i and compactness q the conservation equation reads (for $a = (h_i, q)$:

$$\frac{\partial a}{\partial t} + \vec{u_i} \cdot \nabla (a) = \nabla \cdot (A_i \nabla a) + + F(a) \tag{17}$$

where $\vec{u_i}$ is the ice drift and A_i is a diffusivity, 1 $\mathrm{m^2 s^{-1}}$ $(= A_h)$. The forcing functions F for h_i and q read

$$F(h_i) = -\frac{1}{\rho_i L} Q \tag{18}$$

$$F(q) = \begin{cases} \frac{F(h_i)}{h_{new}}(1 - q) & \text{for } Q < 0 \\ \frac{F(h_i)}{2h_i} q & \text{for } Q > 0 \end{cases} \tag{19}$$

$$\tag{20}$$

where Q is the total heat flux (positive upwards) into the ice, L the latent heat of fusion, ρ_i ice density. h_{new} is the ice thicness for new ice. Based on Mellor and Yamada (1989) and the fact that the horizontal resolution is very high, allowing for thin ice types, we take

[3] here ice thickness is the cell averaged quantity, whereas in the plots below the floe thickness is didplayed, i.e. average thickness divided by q.

$h_{new} = \max[0.1, \min[0.25 \cdot h_i, 0.6]]$. The details about the thermodynamics may be found in [Drange and Simonsen, 1997]

For ice momentum we have

$$\frac{\partial \vec{u_i}}{\partial t} + \vec{u_i} \cdot \nabla \vec{u_i} + f\vec{k} \times \vec{u} + g\nabla\eta = \tau_a + \tau_{oi} + \vec{P_i} \tag{21}$$

η is the sea surface elevation, $\tau_a + \tau_{oi}$ atmospheric and oceanic stress, $\vec{P_i}$ divergence of the internal ice stress P_i which utilize a viscous-plastic rheology according to [Hibler, 1979], with ice strength $P_* = 2000$ Nm^{-1} and $P_i = P_* \exp(20 \cdot (1-q))$

Ecosystem module. The equations describing the dispersion and interaction of ecosystem compartments are given in nitrogen units as:

$$\mathcal{J}(\mathrm{NO_3^-}) = -(G_P - G_{P,\mathrm{NH_4^+}}) + Ox_{\mathrm{NH_4^+}} \tag{22}$$

$$\mathcal{J}(\mathrm{NH_4^+}) = -G_{P,\mathrm{NH_4^+}} + M_P + M_Z + M_D - Ox_{\mathrm{NH_4^+}} \tag{23}$$

$$\mathcal{J}(P) - \frac{\partial w_P P}{\partial z} = G_P - M_P - G_z \tag{24}$$

$$Z = P\frac{Z_{tot}}{\int_{-\infty}^{0} P dz} \tag{25}$$

$$\frac{dZ_{tot}}{dt} = \int_{-\infty}^{0} (G_Z - E_Z - M_Z) dz + S \tag{26}$$

$$\mathcal{J}(D) - \frac{\partial w_D D}{\partial z} = E_Z - M_D \tag{27}$$

where

$$\mathcal{J} = \frac{\partial}{\partial t} + \vec{u} \cdot \nabla_H - A_h \cdot \left(\frac{\partial^2}{\partial x^2} + \frac{\partial^2}{\partial y^2} \right) - \frac{\partial}{\partial z}\left[w \frac{\partial}{\partial z} \right] \tag{28}$$

.

The state variables are $\mathrm{NO_3^-}$, $\mathrm{NH_4^+}$, P, Z, and D, i.e. concentrations of nitrate, ammonium, phytoplankton, zooplankton, and detritus, respectively. The vertical fluxes inherent in the $\mathcal{J}$ operator are assumed the same for all ecosystem variables. G_P is the phytoplancton growth and $G_{P,\mathrm{NH_4^+}}$ its part based on ammonium, M_P and M_Z are metabolisms for phyto- and zooplankton, respectively, and M_D is the bacterial decomposition of detritus. Furthermore, $Ox_{\mathrm{NH_4^+}}$ is oxidation of ammonium to nitrate, G_Z is zooplankton growth, E_Z zooplankton egestion rate, S represents a parameterization of zooplankton transfer from deep to productive layers, and w_P and w_D are the sinking velocities for phytoplankton and detritus, respectively.

An assumption of instantaneous adjustment of zooplankton to the vertical phytoplankton distribution has been made. Furthermore, we will neglect the source term S, and instead specify an initial distribution of Z.

The forcing terms of the system are given as:

$$G_P = \gamma_P \cdot g(T) \cdot I_{lim}(I) \cdot \left(\frac{\mathrm{NO_3^-} + \mathrm{NH_4^+}}{\kappa_N + \mathrm{NO_3^-} + \mathrm{NH_4^+}} \right) \cdot P \quad (29)$$

$$G_{P-\mathrm{NH_4^+}} = \gamma_P \cdot g(T) \cdot I_{lim}(I) \cdot \left(\frac{\mathrm{NH_4^+}}{\kappa_{\mathrm{NH_4^+}} + \mathrm{NH_4^+}} \right) \cdot P \quad (30)$$

$$M_P = \mu_P \cdot g(T) \cdot P \quad (31)$$

$$G_Z = \gamma_Z \cdot g(T) \cdot \left(\frac{P^2}{\kappa_P^2 + P^2} \right) \cdot Z \quad (32)$$

$$E_Z = \varepsilon_Z \cdot G_Z \quad (33)$$

$$M_Z = g(T) \cdot \left(\mu_Z^1 + \mu_Z^2 \cdot Z \right) \cdot Z \quad (34)$$

$$M_D = \mu_D \cdot D \quad (35)$$

$$Ox_{\mathrm{NH_4^+}} = \mu_{\mathrm{NH_4^+}} \cdot \mathrm{NH_4^+} \quad (36)$$

$$g(T) = \exp[b(T - 10.0)] \quad (37)$$

$$I_{lim}(I) = 1 - \exp[-I/\kappa_I] \quad (38)$$

and the numerical values of the various constants are given in Table .

Table 2. Numerical values of constants in the ecosystem model

Constant	Definition	Value
γ_P	Phytoplankton growth rate	1.1 day^{-1}
b	Phytoplankton growth,	0.06° C^{-1}
	e-folding scale for temperature dependence	
κ_I	Phytoplankton growth,	12 Wm^{-1}
	e-folding scale for light dependence	
κ_N	Phytoplankton growth, half saturation	0.1 mmolN m^{-3}
	constant with respect to nutrient	
$\kappa_{\mathrm{NH}_4^+}$	Phytoplankton growth, half saturation	0.1 mmolN m^{-3}
	constant with respect to ammonium	
μ_P	Phytoplankton metabolism	0.03 day^{-1}
w_P	Phytoplankton sinking rate	1 m day^{-1}
γ_Z	Zooplankton growth rate	1.1 (mmolN m^{-3})$^{-1}$ day^{-1}
κ_P	Zooplankton growth, half saturation	0.5 mmolN m^{-3}
	constant for feeding on phytoplankton	
ε_Z	Coeff. for zooplankton	0.2
	sloppy feeding	
μ_Z^1	Coeff. in zooplankton metabolism	0.2 day^{-1}
μ_Z^2	Coeff. in zooplankton metabolism	0.2 (mmolN m^{-3})$^{-1}$ day^{-1}
μ_D	Bacterial degradation of detritus	0.3 day^{-1}
w_D	Detritus sinking rate	1.0 m day^{-1}
$\mu_{\mathrm{NH}_4^+}$	Bacterial oxidation of ammonium	0.04 day^{-1}

The defaults from [Broström and Drange, 2000] are $\kappa_I = 10$, $\kappa_P = 1.5$, $\mu_Z^1 = 0.05$, $\mu_Z^2 = 0.15$, $w_D = 10$ (in addition to w_P being finite only in the ML, 0 else)

Experiments

We have studied several cases of combination of wind scenarios and eddy development. Here we show results from three cases: One with a wind blowing with the ice to the right (a typical siuation), one withe the opposite. The latter is atypical but leads to a better understanding e.g. of situations with passing low-preessure systems when the wind can turn 180°. For completion we also incude a case in which the wind is turning 360 °.

Lay-out. In order to resolve the internal Rossby deformation radius R_d, estimated to 3.5 km, the model is set up with a horizontal resolution of 500 m. The situation in the Fram Strait at 80° N is resembled roughly: A rectangular channel is applied, with the upper half covered with sea-ice. The channel is periodic in the along wind direction (with ice to the right for basic case) and use closed walls for the "sides", which are placed far away from the dynamically active MIZ, such that negligible influence from the sides is noticed. The ice is set

to 1.08 m thick and 0.99 concentration at the inner MIZ, both falling linearly to zero over the outer 5 km.

The ocean is composed of only 3 layers, with the ML subdivided into 2 layers for the ecosystem model. The layers no. 2 and 3 from above has sigma-theta fixed to 27.11 and 27.36, respectively. The deepest layer extends to 1000 m and hardly interacts with the upper ocean. The large depth is thus not justified when looking at upper ocean response, but is nevertheless included for future applications. The extra computational cost implied by the need for short time steps due to the rapid external mode, is not unbearable.

Initialisation. The initial fields are – in accord with the layout – idealized, cf. Table . We take initial thicknesses to be constant, as well as the upper layer pot. density. Thus we do not prescribe any frontal structure and aim at pure baroclinic response of the interfaces. However, we specify the open ocean salinity gradient as 0.004 km^{-1}, and impose a density compensating temperature. The ML thickness, 21 m, is in accord with observations, although the stratification below yields somewhat too weak stability than observations. The choice is thus more applicable to a winter situation, during which ice-edge up-welling is more likely to occur.

Table 3. Initial conditions. Note: The BGC compartements have a decaying concentration in the ice covered part. The ML is subdivided into 2 bio-layers; both has the Layer 1 values.
*) Temperature is set to freezing in the ice covered part and calculated from salinity and density in the open ocean.
**) Salinity is constant in the ice covered part and having a gradient 0.004 km^{-1} in the open ocean.

Layer #	h [m]	T [° C]	S	NO_3^-	NH_4^+	P	Z	D
1	21.0	*)	33.00**)	2.5	0.0001	2.5	0.08	0.0001
2	71.0	1.32	33.84	10.	0.0	0.0	0.0	0.0
3	908.0	2.73	34.29	10.8	0.0	0.0	0.0	0.0

For the bioogeochemical module the upper layer (i.e. bio-layers 1 and 2) is initialized with 2.5 mmolN $m^{-3}$for both NO_3 and phytoplancton in th eopen ocean. For these values the nitrate is consumed within 2–3 days, so that the system is nutrient limited and a strong signal from physical effects (entrainment) can be noticed. For zooplancton, ammonium and detritus there are small background values. In the bio-layer 3 [NO_3] is set to 10.0 mmolN m^{-3}, a maximum figure in accordance with observations. The concentrations of the biogeochemical compartements in the ML decay iceward from the ice-edge with an e-folding scale of 5 km. The exception is NO_3^-which is homogeneous throughout the ML, thus the under-ice region will act as a pool for of nutrient, as can be inferred from typical MIZ nutrient sections [Sakshaug *et al.*, 1992].

Initially the physical state is perturbed by a "wave-packet" consisting of a wavenumber

2 disturbance of the pressure field in y with a bell shaped modulation both in x and y with e-folding scales in x with e-folding scale 6.5 and 12.5 km, respectively. The amplitude is 8 m at the channel center in both layers 1 and 2. Thus initially at about 20 and 30 km (y-distance in the figures) there is an anticyclone and a cyclone present with 29 and 13 m ML thickness, respectively. As the wind is ramped up, these features propagate down-stream. The exact characteristics of the initial disturbance is not of interest at this stage; here it is used to imply along-wind inhomogenities in order to induce 3-D variability.

Forcing. For the wind forcing we specify a dynamically determined wind stress according to [Guest *et al.*, 1995] as described above. Thus the geostrophic wind has to be specified. First, for all cases the wind has no along channel variation. Second, the cross-channel structure denotes a uniform wind vector over the central half of the channel while tapering off to nil at the closed boundaries, in order to minimize interior influence of boundary effects. The remaining factor is its time-component, which will be described below.

The atmosphere is further simplified with the ocean relaxing to a specified atmospheric temperature, implying an upward heat flux according to

$$Q = 1.84 \cdot W_{eff} \cdot (T - T_a) \tag{39}$$

where $W_{eff} = r \cdot W + 1.0$ from Eq. 2 Thus we collect all heat flux components into a single "sensible" flux, recalling that the turbulent heat fluxes have the strongest feed-back factor. The specified temperature is set to -11° C at $x = -50$ km, increasing to T_f at $x = 0$, and $T_a = 5°$ C at $x = 50$ km. The ocean is thus warmed with $\sim$10 Wm^{-2} over the open ocean, and a corresponding cooling over the ice. The profile of T_a is fixed in all experiments. The evaluation of heat fluxes is described in the main reference. A final remark on the validity of the assumption of non-divergent conductive heat flux in the ice is timely: As we only prescribe smooth transitions in the atmospheric forcings, there is little effect of the buffering of heat storage in the ice, apart from the fact that the dominant heat transfer on the ocean eddy-scale is the one due to ice melt (refreeze) in open (freezing) ocean.

The insolation is simplified to only affect biological growth, and not ocean temperature, for simplicity. The light is simply "switched on" at simulation start, with daily mean insolation for mid-summer at 80° N and 50 % cloud cover. The insolation is attenuated by ice concentration, and with an extinction depth for the ice of 1 m.

Basic case with interactive ABL and on-ice wind; ITR

In this reference case the wind is ramped up to full speed of 10 ms^{-1}, from day 2 till day 3, ramped down to zero between days 5 and 6. The direction is from the right in the figures (on-ice in terms of Ekman transport). The immediate effect of switching on a wind is that the surface ice or ocean is accelerated to large magnitudes $\sim$0.2 ms^{-1}. An upwelling signal at the ice edge is induced, along with a downwelling under the ice within a few R_d (Fig. 2, upper panel). The structure of the pressure field is modulated by the initial perturbation.

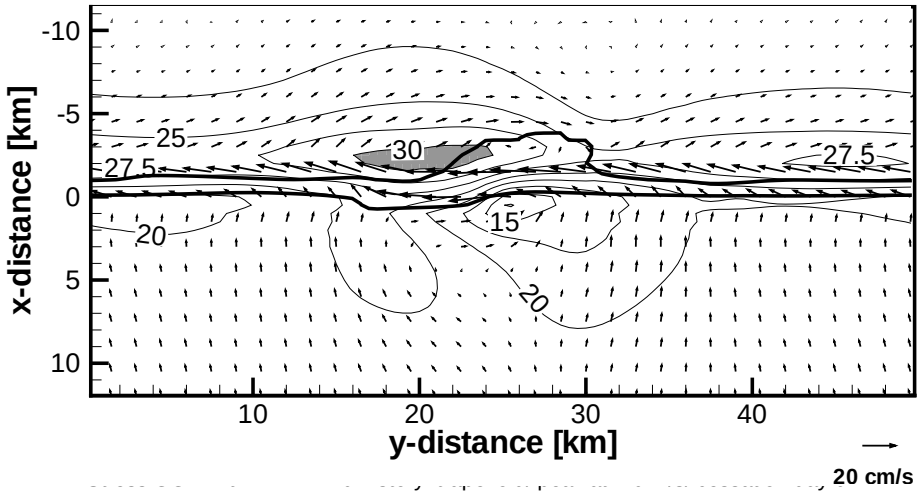
x-distance [km]
y-distance [km]
-10
-5
0
5
10
10
20
30
40
25
27.5
30
27.5
20
15
20
20 cm/s

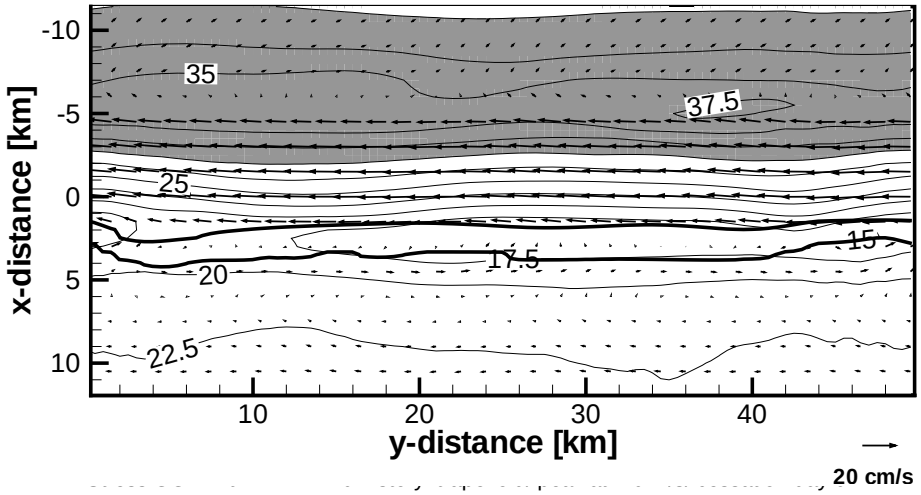
x-distance [km]
y-distance [km]
-10
-5
0
5
10
10
20
30
40
35
37.5
25
15
17.5
20
22.5
20 cm/s

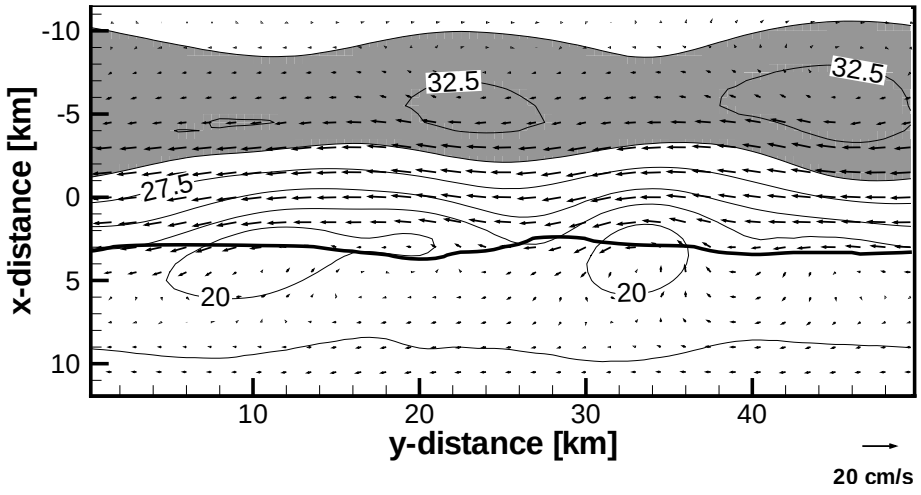
x-distance [km]
y-distance [km]
-10
-5
0
5
10
10
20
30
40
32.5
32.5
27.5
20
20
20 cm/s

Figure 2. Basic case at $t = 3$ days (upper), 6 (middle)10 (lower): Mixed-layer depth [m]and velocity vectors. Thick contour: 20 % ice iso-line.

Due to the compact inner MIZ, the stress on ocean is vanishing, thus there is a convergence just inside the ice, iceward of the stress maximum. This leads to a marked downwelling region, setting up a slight geosrophic counter-current under the ice. At the open ocean side cyclonic counterparts of the anticyclones are found.

At $t = 6$ days, both up- and down-welling signals have strengthened slightly; the 22.5 m contour has approached ice-ward, implying that, over-all, entrainment is slightly stronger than the upwelling over the open ocean (Fig. 2, mid-panel). This may explain the sustained abundance of phytoplankton (see below). The initial cyclonic eddy has reached the channel opening (propagated 30 km in 3 days) maintaining its strength slightly, as a result of cyclonic vorticity input from the wind-stress shear. Even if there is a strong stress gradient, implying upwelling, at the ice edge, the integrated effect of an iceward Ekman drift with a cessation under the fast ice creates a convergence and downwelling to dominate. The downwelling anomaly is about 17 m, while the corresponding upwelling is less than m.

The ice is rapidly adjusted to the wind field (Fig. 4), with down-wind speeds of about 0.20 ms^{-1} rather uniformly over the MIZ. The ice edge is responding to the strong cyclonic eddy located at the channel opening. Another marked feature is the demonstration of the sea surface tilt (not shown) resulting from the pile-up by wind in governing the ice: The ice cover extends about 4 km into the original open ocean due to the down-slope effect, even if the wind is working oppositely.
The on-ice Ekman transport compacts the ice further; this leads to a narrowing of the region of stress-maximum and thus to a weakened ice-edge upwelling.

After 4 more days (Fig. 2, lower panel), the wind being quiet for 3 days, the ice jet system becomes unstable, and the cyclones are seen to maintain its structure — although elongated, while the anticyclones are somewhat more damped out. Note also that the signature of cyclones have the original absolute ML htickness, while they are anomalous relative to the new over-all MLD for the MIZ. The down-stream portions of the cyclones are capable of exchanging material between MIZ and open water.

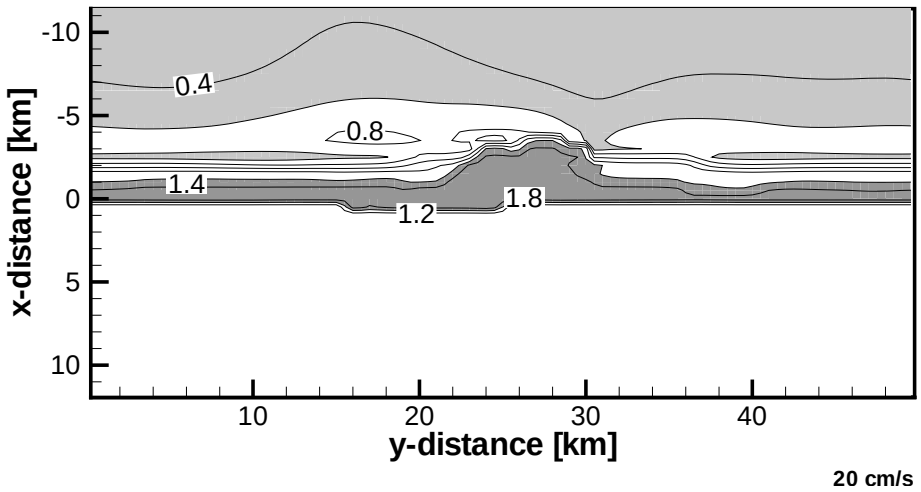

Figure 3. Basic case at $t = 3$ days: u_* [cms^{-1}]Thick contours: 20 and 80 % ice iso-lines.

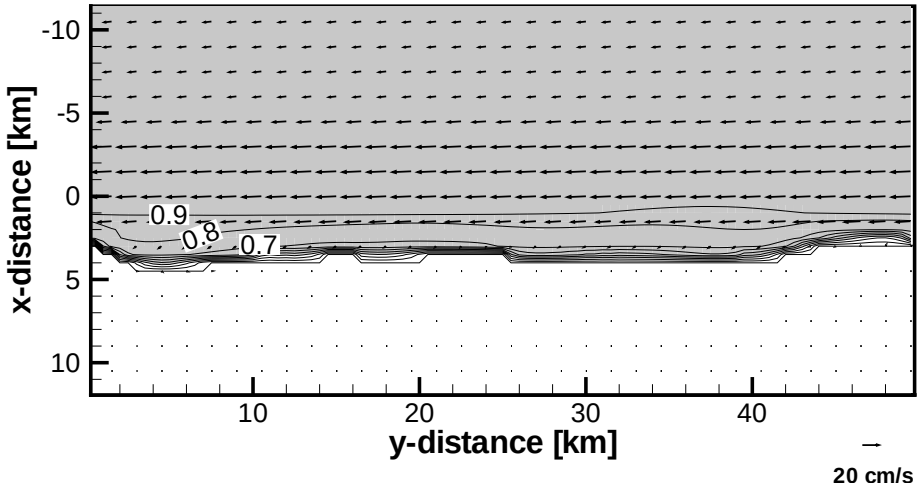

Figure 4. Basic case at $t = 6$ days: Ice concentration[ ] and velocity vectors

Ecosystem. The phytplankton is initially wihtin a culminating bloom phase. The wind is pushing water under the ice with the phytoplankton being advected with it. Thus at $t =$ 3 days the gross view depicts a cross-edge gradient in P reflecting the light inhibition factor (Fig. 5, upper). The weak spatial structure mainly reflects the initial state; e.g. the elongated feature from $y = 0$ to $y = 25$ km iceward of the 80% contour, is a remnant of the initial off-ice advection of low-concentration P and NO_3^-.

At $t = 10$ days the wind has been quiet for 4 days, and the ecosystem is in a new quasi-equilibrium state. The cross-ice gradient in P persists, while its absolute values are somewhat lowered relative to $t = 6$ days. The nitrate has been consumed from the initial state, but has not become a limiting factor in the open water at $t = 6$ days, with values above 0.6

mmolN m^{-3}(Fig. 6, upper). The pattern is broadly anticorrelated with that of P. There is also some upwelling signal inside the ice, due to the slight admixture of lower-layer properties due to the elevated mixing due to the moving ice.

At $t = 10$ days (Fig. 6, lower) the open wate rhas become devoid of NO_3^-, while the ice covered region maintains its elevated figures, due to the ice-water stress, maintaining mixing.

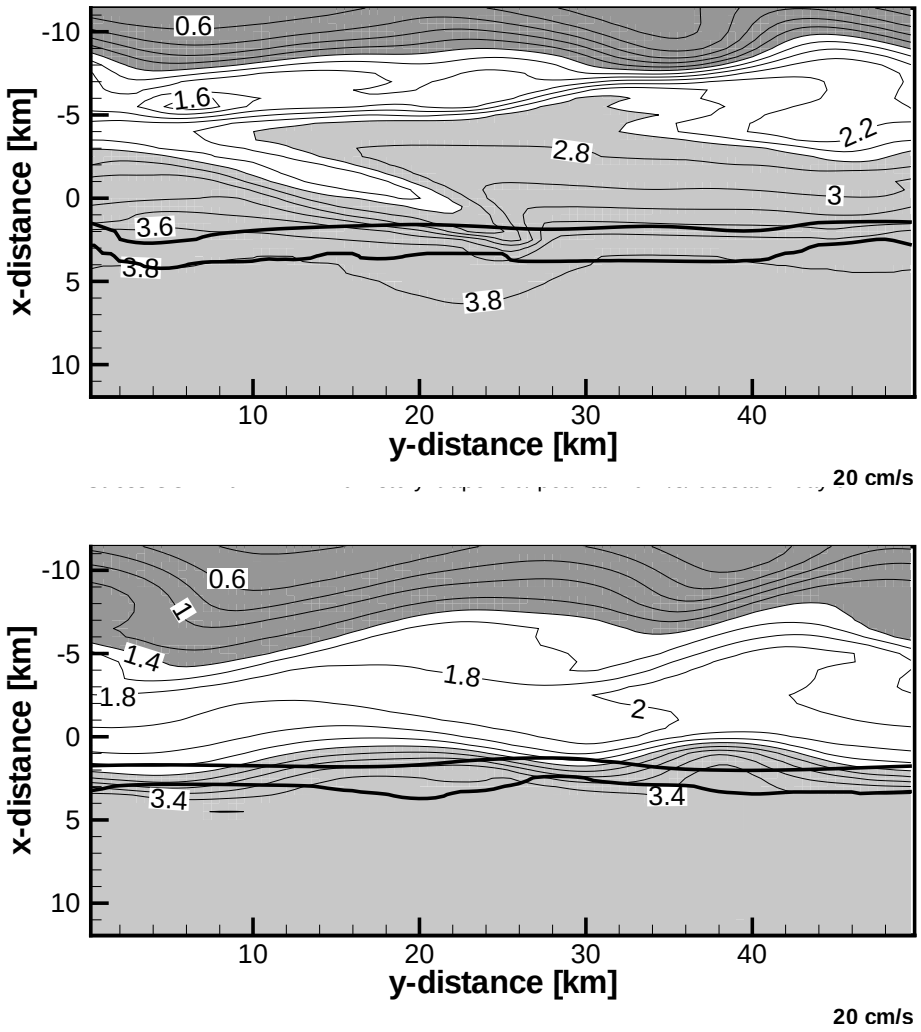

Figure 5. Basic case at $t = 6, 10$ days: Phytoplankton mmol m^{-3}

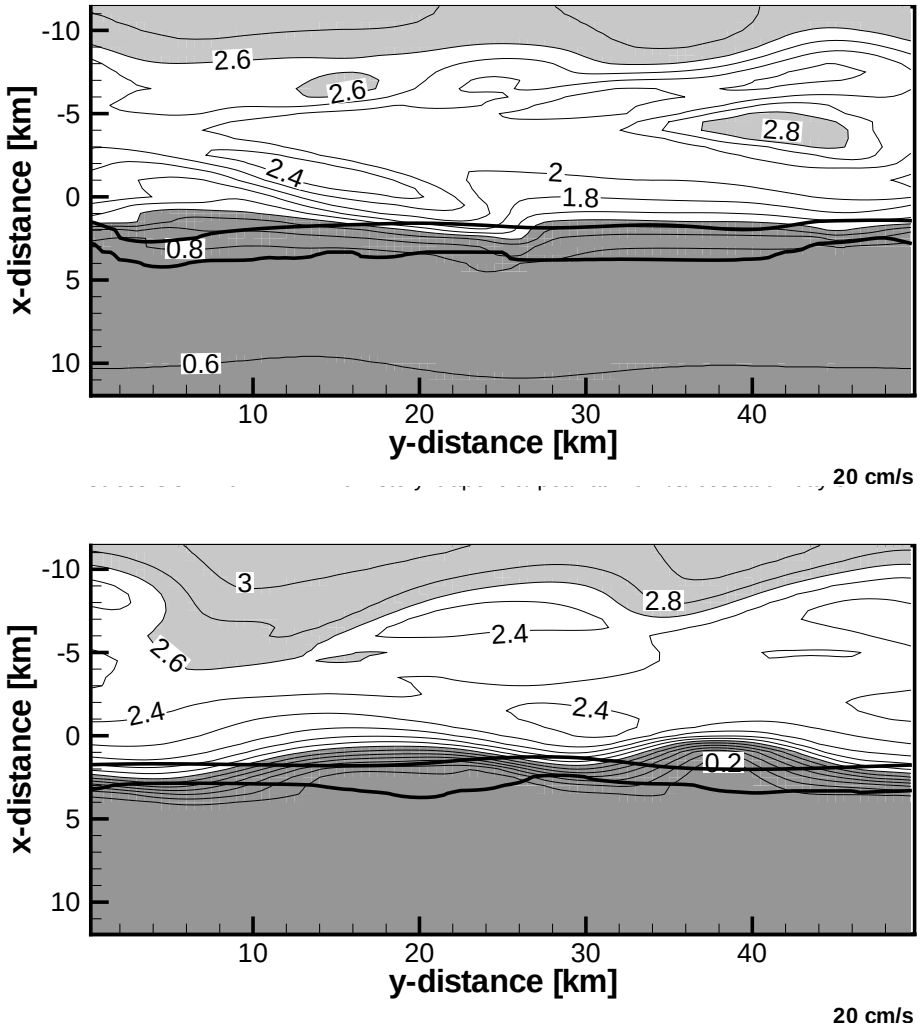

Figure 6. Basic case at $t = 6, 10$ days: NO_3 mmol m^{-3}

The new production is strong (but not unrealistic) in the open water due to light and nutrients (Fig. 7). Inside the ice it is lower, implying an advective source for the phytoplancton, rather than growth . Even if there is strong upwelling near the ice edge, the water is also advected under the ice, so the extra surplus cannot be utilized fully. The regenerate production is small all-over, due to the small initial presence of ammonium (Fig. 7), even if a gradient from ice to open water is present.

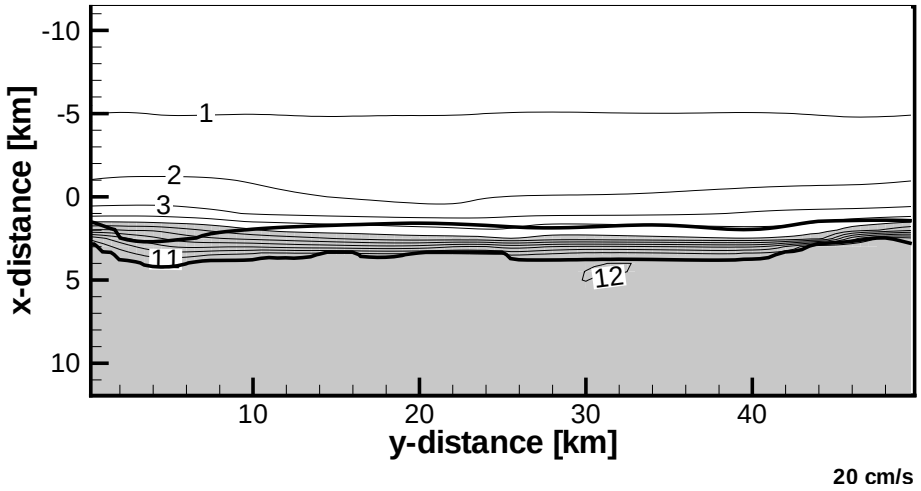

Figure 7. Basic case at $t = 6$ days: New production mmol m^{-2} d^{-1}

When the wind has ceased the system evolves slowly. On day 10 some small cyclonic eddies (5 km in diameter) have developed on the open-water side of the ice-edge jet, while the open water starts to get devoid of nitrate. Thus there is a stark contrast in new production from nutrient rich to nutrient poor areas. 7. Maximum new production is 5–9 mmolN $m^{-2}d^{-1}$iside these features with a regenerate production of 5 mmolN $m^{-2}d^{-1}$(Fig. 9), making a total maximum primary production of 14 mmolN $m^{-2}d^{-1}$. The background values in the open water are 0.5 and 5 mmolN $m^{-2}d^{-1}$, respectively, indicating that the nitrate is consumed and that the phytoplancton is maintained by light and a small supply of nitrate entrained from below. (This corresponds to the presence of the deep phytoplankton maximum in a model with higher vertical resolution). A few kilometers inside the ice-edge, however, the nitrate concentration is reaching 2.5 mmolN m^{-3}, reflecting a pool of nutrients being unaffected by consumption under the shadowing ice. The growing cyclones advect nitrate from the MIZ into the open water, maintaining the production maxima there.

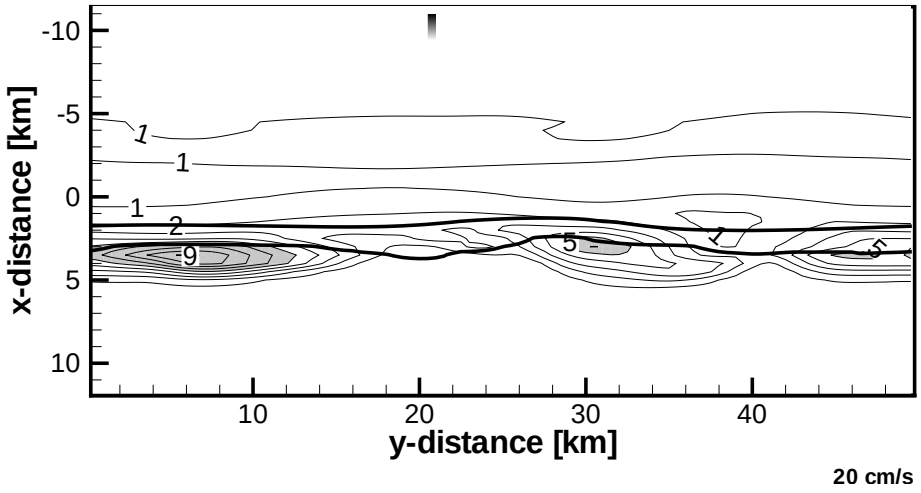

Figure 8. Basic case at $t = 10$ days: New production mmol m^{-2} d^{-1}

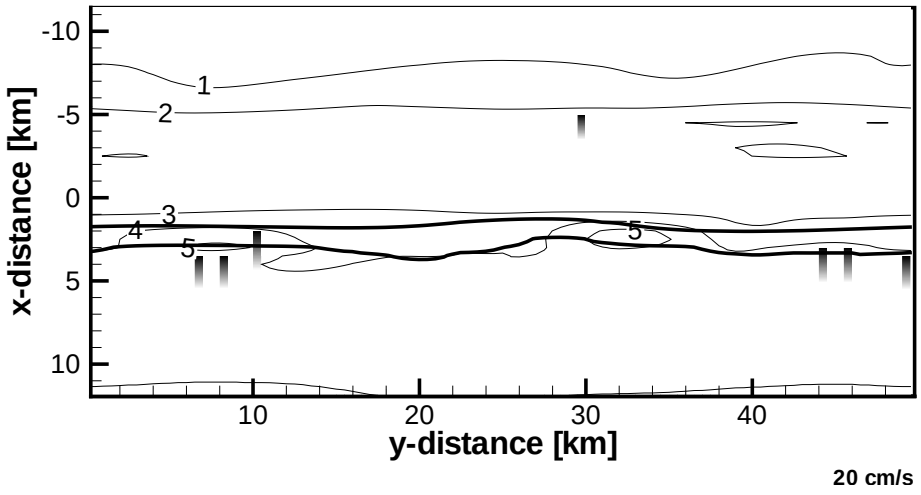

Figure 9. Basic case at $t = 10$ days: Regenerate production mmol m^{-2} d^{-1}

Wind blowing with ice to the left; ITL

In this case the Ekman transport is off-ice, leading to a piling up of ML outside the ice edge, everything else the same as in the reference case (Fig. 10, upper. Moreover, as the MIZ diverge, the area with enhanced stress is broadening, leading to a positive feedback to the off-ice transport. Hence, the ML deepening (and shoaling inside the compact ice) is comparatively more pronounced than in the reference case. The ice-edge jet which is set up is stronger and destabilize more rapidly. A street of anticyclones of 15 km diameter form in the strong shear zone at the ice edge (Fig. 10, middle). At $t = 10$ days the anticyclones have strengthened and evolved into vortex pairs with smaller cyclones on their ice-ward sides

(Fig. 10, lower). Two of the anticyclones have merged into a larger (slightly asymmetric) structure located at the channel opening.

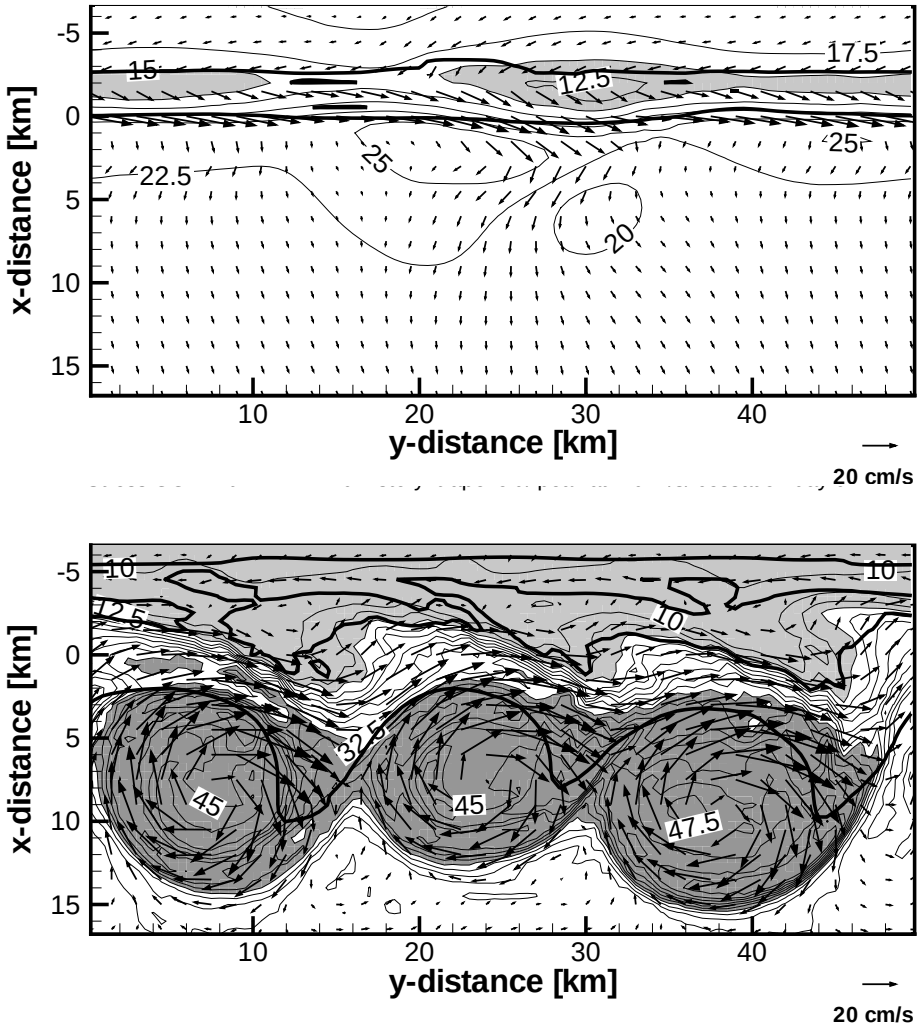

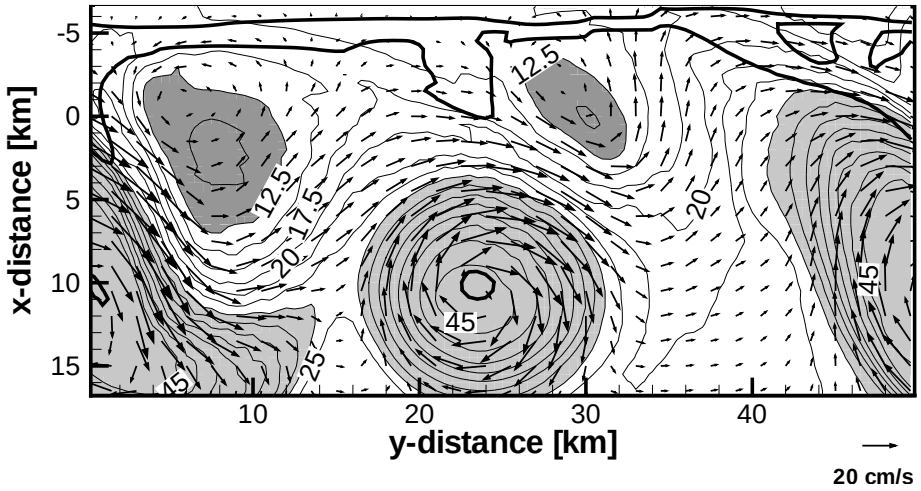

Figure 10. Off-ice case at $t = 3, 6, 10$ days: Mixed-layer depth [m]and velocity vectors

The u_* for the ITL case has slightly broader extension than the ITR case, denoting that the MIZ is in the course of expansion.

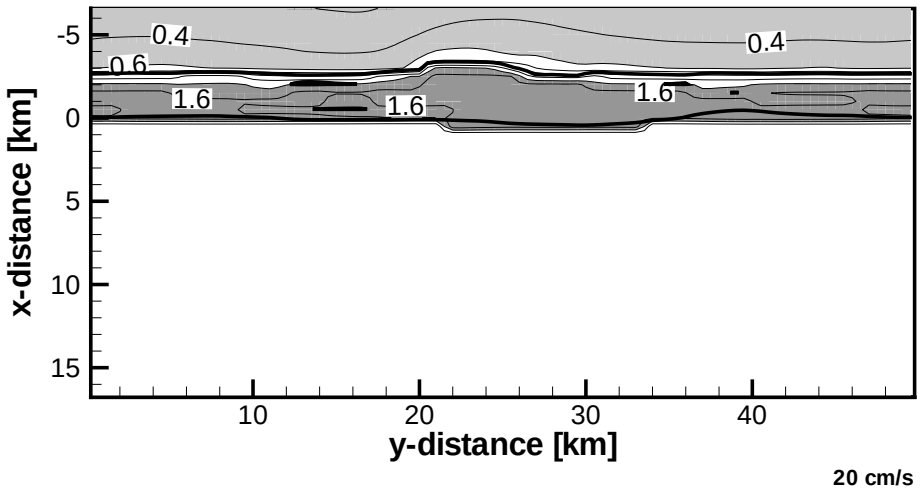

Figure 11. ITL case at $t = 3$ days: u_* [cms^{-1}]Thick contours: 20 and 80 % ice iso-lines.

Also the ice shows strong variability with long bands of ice shooting out from the inner MIZ, coherent with the vortex pairs (Fig. 12). As a light limiting factor the ice has strong influence on the spatial variability of phytoplankton. Moreover, there is an ice concentration minimum evolving outside the "old" pack ice, in association with the strong upwelling.

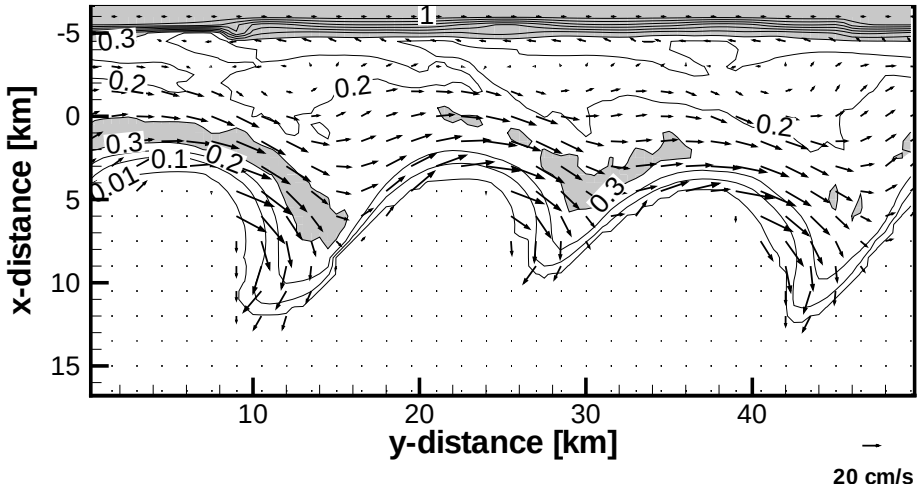

Figure 12. Off-ice case at $t = 6$ days: Ice concentration [ ]

Ecosystem. The phytoplancton concentration depicted at day 6 (Fig 13, upper) shows that the initial cross-edge gradient is deformed by the eddies, and that the lower value P is over shadowed by medium ice concentration. Indeed, the entire MIZ system is shifted outwards, denoted by the comparably low values of P (< 0.4) in the inner upwelling zone. Phytoplankton rich, nitrate poor waters from the open ocean is similarly advected by cyclones under the ice, reducing growth.

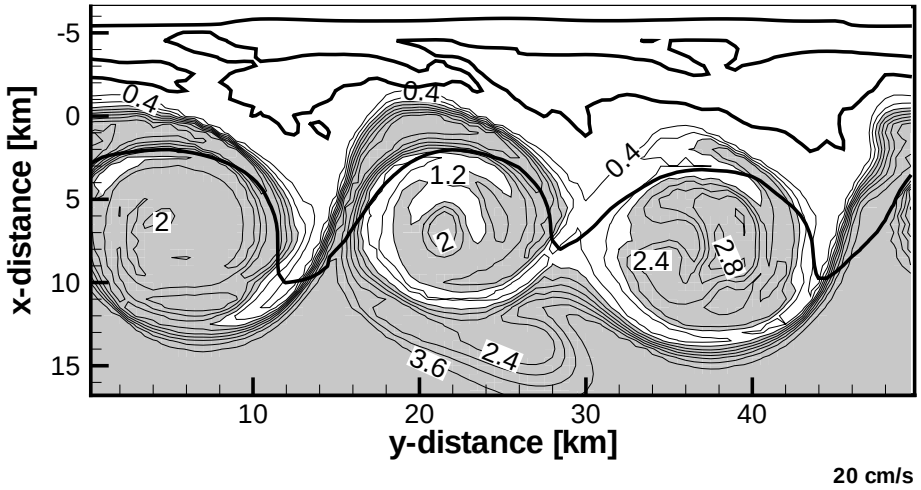

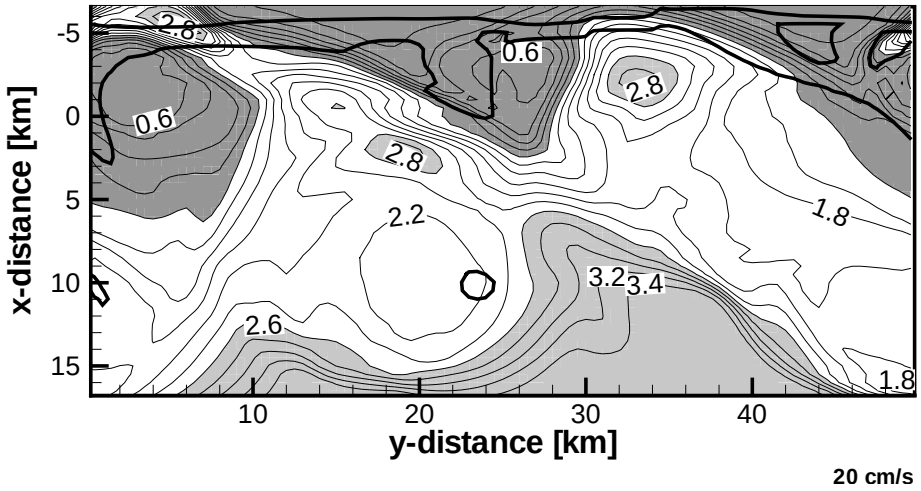

Figure 13. Off-ice case at $t = 6, 10$ days: Phytoplankton mmol m^{-3}

For the nitrate the increased stress (mixing) in combination with upwelling near the inner MIZ edge, lead to strong surplus of nitrate (Fig. 14, upper) which is subsequently captured by the evolving eddies and lead to the open water. The maxima of new production (Figs. 16 and 15) are found in the open water and – secondarily – in the ice-free portion of the central anticyclone which has sufficient nutrient abundance and has been exposed to light long enough. The depleted values in new production extending out from the ice curled up by the eddies simply reflects the P distribution, i.e. a scaling effect due to the lower P values inside the ice. NO_3^- is superfluous in th eentire domain.

At 10 days near ice-edge maxima in new production are manifest (Fig. 16). These correlate with the upwelling structures associated with the cyclonic companions of the (larger) anticyclones. The origin of the maxima are the advection of P poor, NO_3^- rich water out from the dark ice region. The co-acting effects of upwelling and increased light exposure due to horizontal advection both enhances growth. Similarly, the production is lowered again when the water mass is re-injected under the ice. There is also a contribution to elevated growth from advection of water from the open region which has elevated P, malking the exact distinction between the horizontal surplus of "new" waters from the ice and the "old" open waters difficult.

In the open water the growth is in the way of being NO_3^- limited, as well as in the centers of the anticyclones where the water column is thick (light inhibition) and where again new production correlates with P.

Wieved in the light of its ITR counterpart, the ITL case shows a similar behaviour close to the "old" ice edge: Cyclones exposing the nutrient rich ice water to light. The effect is larger due to the stronger mechanical energy input, causing stronger upwelling (light exposure) and larger eddies (prolonged exposure time). The anticyclones of the outer region further transport and mix horizontally the nutrient rich water mass outwards, partially counteracted by inmixing of nutrient depleted waters from the open ocean originally unaffected by eddy

activity, as well as the light-inhibition effect at the eddy centers where there is some stagnation. If the evolution were to be followed further in time, one should suspect the high bioactivity in ring-structures surrounding the weakening anticyclones and in patches along the ice edge.

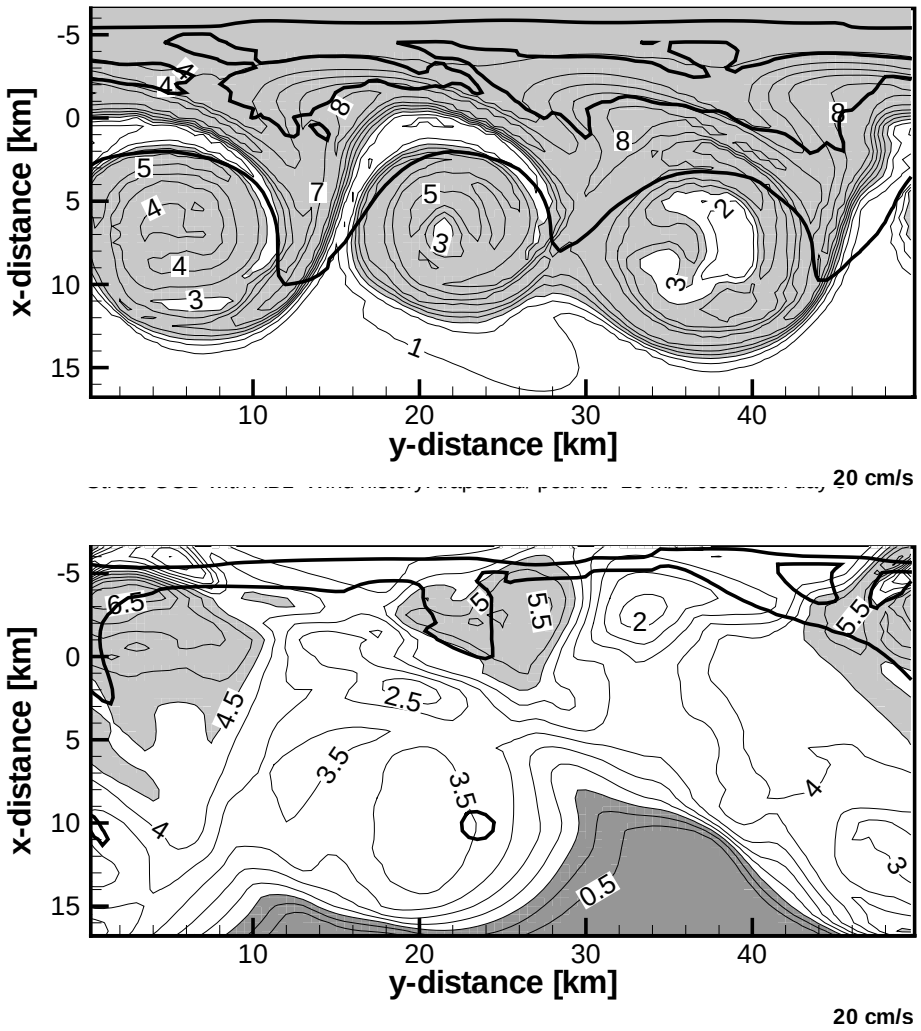

Figure 14. Off-ice case at $t = 6, 10$ days: NO_3 mmol m^{-3}

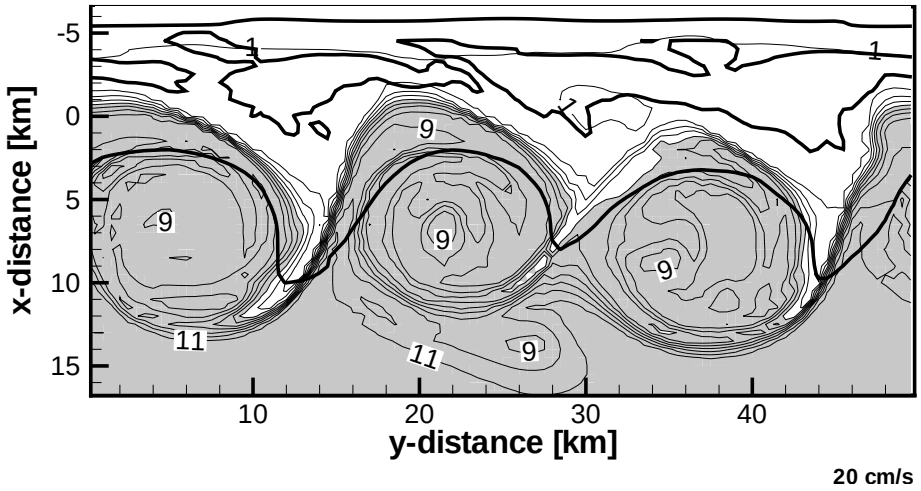

Figure 15. Off-ice case at $t = 6$ days: New production mmol m^{-2} d^{-1}

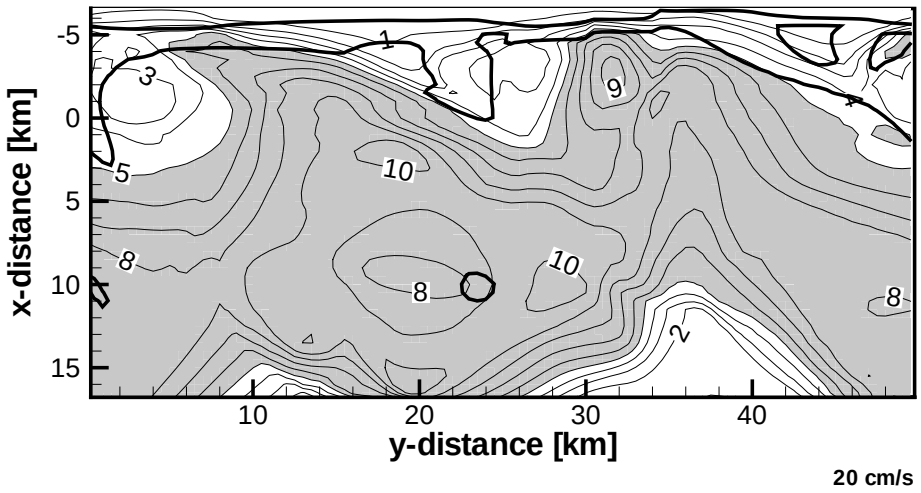

Figure 16. Off-ice case at $t = 10$ days: New production mmol m^{-2} d^{-1}

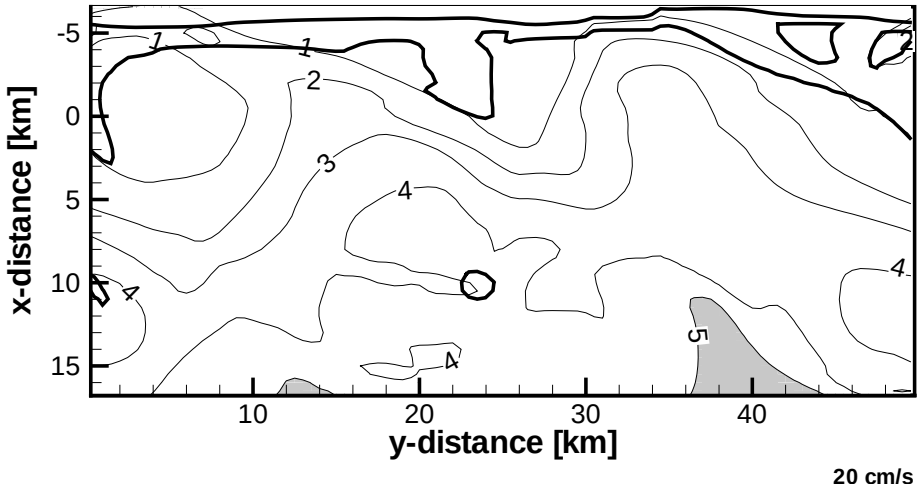

Figure 17. ITL case at $t = 6$ days: Regenerate production mmol m^{-2} d^{-1}

Quantifying the effects of the eddies

In order to evaluate the significance of the eddies, we performed two virtually 2D experiments in which there was no along edge variability. Otherwise the experiments were the same as the basic ITR and ITL cases. In Fig. 18 the half-basin average phytoplankton concentration is shown. It is clear that in the ITR case there is only a negligible increase in concentration for the eddy case. It is rather showing a delay of the bloom, which is consistent with the 3D pattern as described previously.

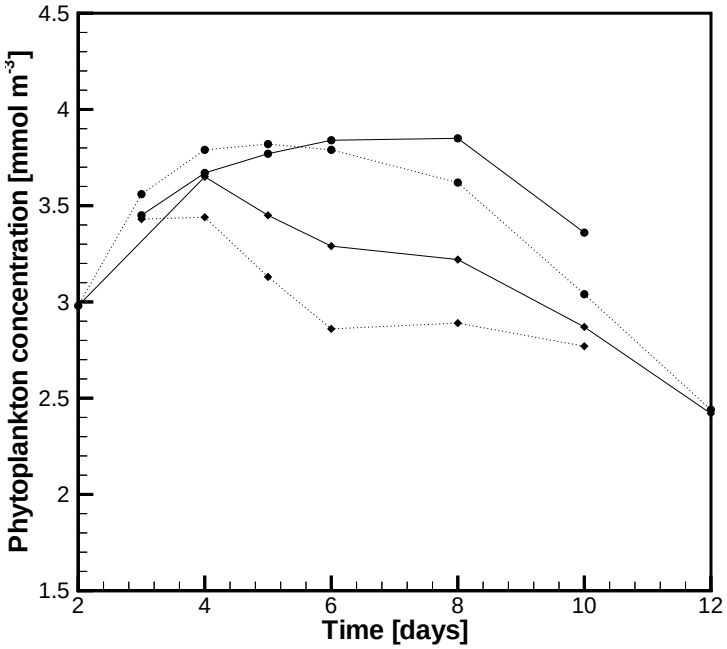

Figure 18. Time development of open ocean average phytoplankton concentration.Full line: 3D cases; dotted line: 2D cases; circles: ITR cases; diamonds: ITL cases.The averaging area is for $0 < x < 28$ and along channel.

For the ITL cases there is a more persistent difference in concentration, the 3D case showing 10–20% higher values. The earlier decay of the bloom for these cases is due to both the deepening of the ML along the ice edge andthe ice advancing beyond $x = 0$. Averaging over the ice free domain would have shown less decay. The subtle balance of eddy advection both bringing water masses of low concentration out in open water and the opposite comes out with a net positive effect.

The primary production is consistent with these findings: The new production, Fig. 19, for the ITL cases is decaying earlier than for the ITR ones. During the final stage, however the new production goes to zero for the ITR cases due to nitrate exhaustion, as pointed out previously and as will be shown in the following. The regenerate production is very similar for all cases. We also show a plot of phytoplankton versus nitrate, in order to eliminate the effect of different timing of the bloom for different cases. Most prominent is the emptying of the ML of nitrate for the ITR cases after about 10 days. For the ITL cases, on the other hand, after an initial consumpiton of nitrate, there is a large increase during the wind event between day 4 and 6, which is due to the pumping of new nutrient from the upwelling area inside the MIZ. The increase for the 3D case is only about half of that of the 2D case, a fact that again can be ascribed to the "smearing out" effect of the eddies. In the former case the nitrate concentration is kept approximately constant around 1 mmol m^{-3} for the days 8–12, while the 2D case show decay iin nitrate. Hence, the eddies in the early stage evens out the nitrate concentration, while later on they can sustain nitrate supply so that new production is kept at a significant level (Fig. 19).

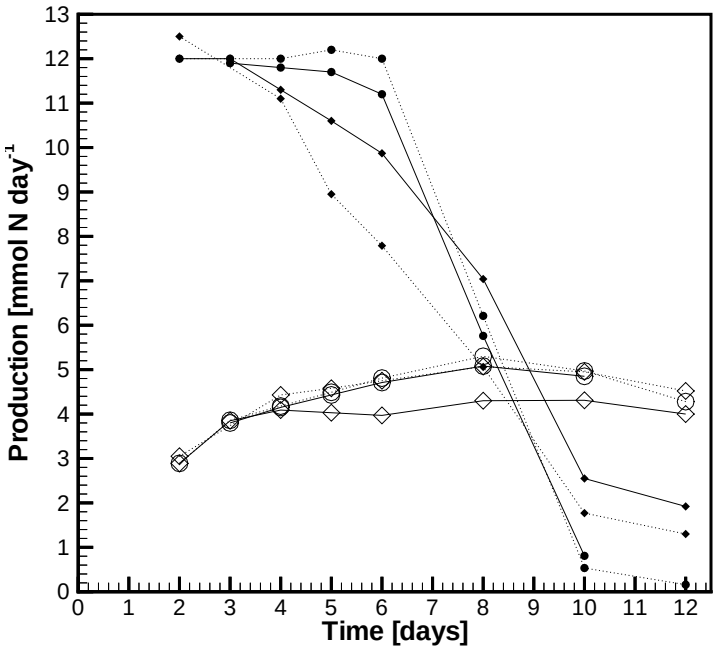

Figure 19. Time development of open ocean average new production (filled symbols) and regenerate production (large open symbols).Otherwise as Fig. 18.

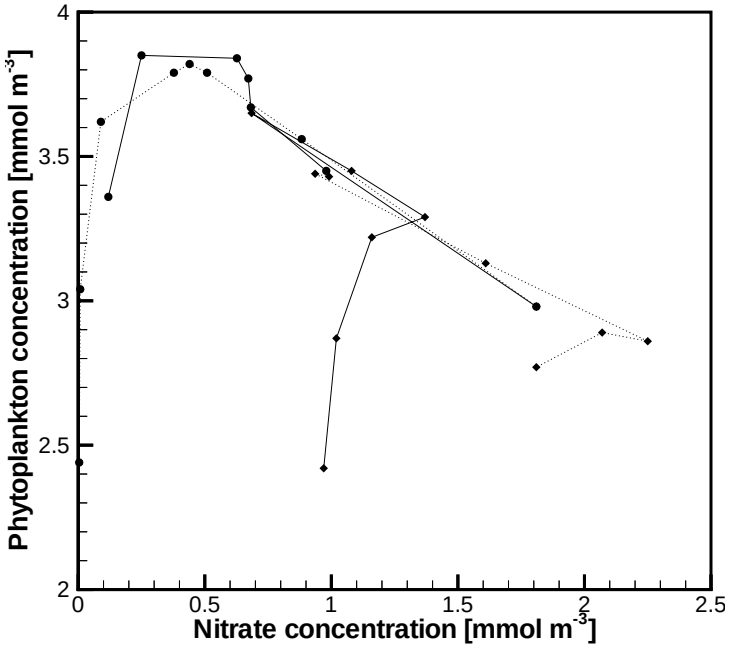

Figure 20. Time development of open ocean average phytoplankton concentration vs. nitrate concentration.Otherwise as Fig. 18.

Wind episode of wind turning 360 degrees within 2 days

To determine the relative effect of the roughness–expansion feedback and the presence of along-ice inhomogenities, we superimposed the basic ITR case with a wind component turning and attenuated in a way such that it is zero at $t = 3$ days, pointing off-ice at 3.5 days, opposite to the bakround wind and at maximum at 4.0 days and zero again at 5 days. Outside this time interval there was no rotating component, i.e.

$$|w_{rot}| = w_{max} \sin(\frac{\pi t}{T_r}) \quad (40)$$

$$\theta_{rot} = \frac{2\pi(t - t_0)}{T_r} \quad (41)$$

where t_0 is 3 (days), $T_r = 2$ days, and θ is clockwise from the x-axis. $w_{max} = 20$ ms-1 is chosen such that the total wind is directly opposite in magnitude and direction to the background at half period. Here we show only the situation at 10 days for the most relevant quantities.

The sytem is in a ITL phase around day 4, during which the ice expands markedly outwards. In other respects the situation is very similar to the ITR case. At day 10 (Fig. 21) the pressure field has the same small eddy structures reciding at the ice-edge. Apart from the ice edge being shifted about 9 km outwards relative to the basic case, the eddies are somewhat

stronger, providing more light in the ML and strong advection of nutrients. The growth of anticyclones is absent because of the already compacted ice edge and the precence of cyclonic vorticity which has to be overcomed. During the ITL phase there seems to be an energizing of the already present patterns dominated by the ITR conditions. Note also that the magnitude of the total wind-speed exceeds the original maximum, increasing u^* and over-all entrainment accordingly.

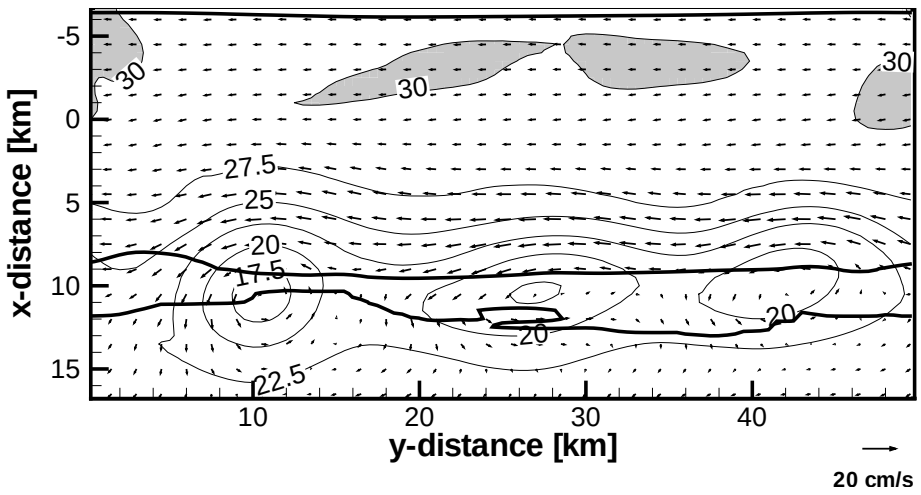

Figure 21. Turning wind case at $t = 10$ days: MLD [m]

The nitrate is slightly enhanced under the ice relative to the basic case at 10 days, due to the extra pumping during the ITL phase. Note also that in association with with the largest eddy ($x = 0, 10$) the high concentration region is brought into contact with the MIZ, preconditioning an extended bloom.

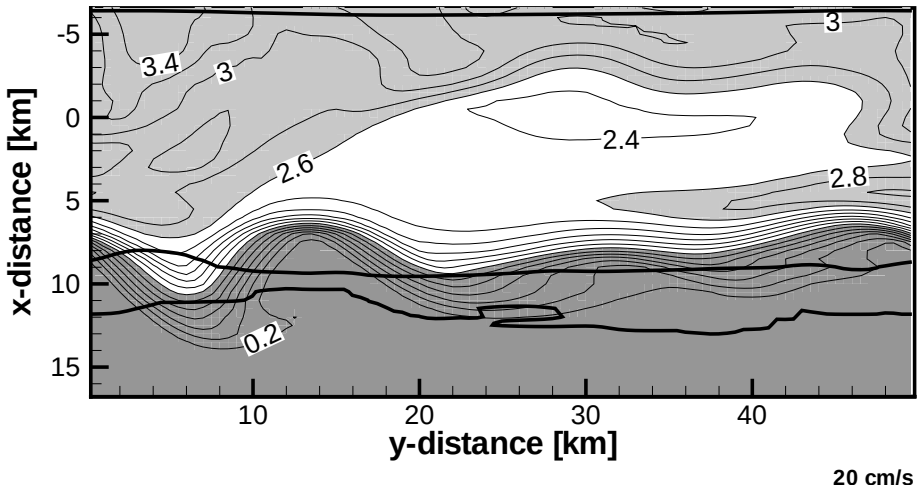

Figure 22. Turning wind case at $t = 10$ days: NO_3^-[mmolN m^{-3}]

The implied production is slightly elevated within the eddies, with larger amplitude and extension in accordance with the eddy strength.

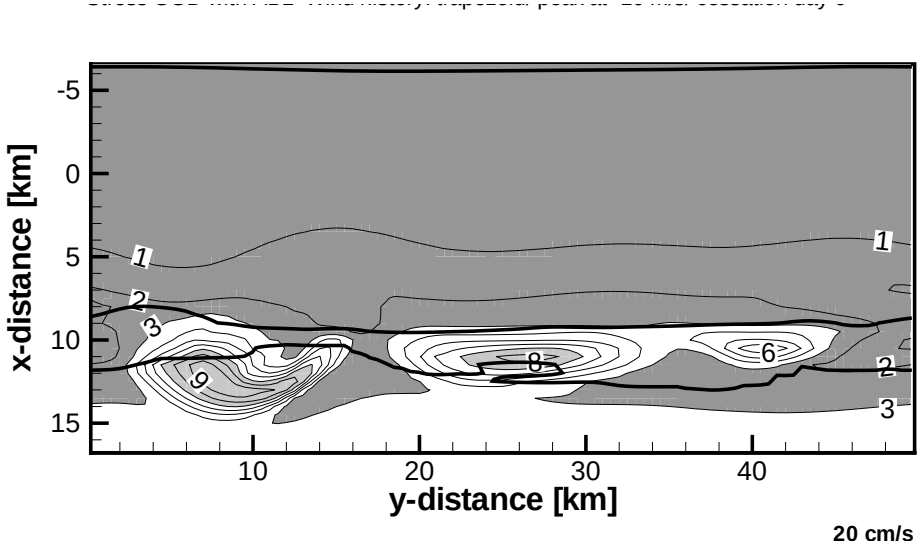

Figure 23. Turning wind case at $t = 10$ days: New production [mmol m^{-2} d^{-1}]

Discussion and conclusion

The two cases with along ice winds share some common features, despite the wind direction and immediate ocean response. In both cases the implied up- or downwelling zones were small (10–20 km) and biologically insignificant compared to the "infinite" open ocean, a finding in common with the 2-D study of [Niebauer and Smith, 1989]. In an ocean void of nutrients in the ML, the contrast between open ocean and MIZ would be marked, however. During an up-welling situation nutrients are brought towards the surface for consumption, while during downwelling a region with beneficial light and nutrient conditions is created as the MIZ diverges, also promoting production. A rapid break-down of the ice-edge jet system into eddies – cyclones in the ITR case and anticyclones in the opposite case – enhances primary production: at the off-ice sides of the cyclones nutrient rich water is brought into the open water, and at the rims of the anticyclones the nutrient concentrations is high enough and the ML depth shallow enough to optimize growth. We did not extend the simulations in order to investigate the spin-down of our eddies, but life times are likely of the order of weeks ([Johannessen *et al.*, 1987] estimated the life time of Fram Strait eddies to about 2 months for eddies somewhat larger than here).

In this view, the familiar notion of episodic supply of nutrients due to stirring by passing lows can now be reinterpreted: Rather than a simple 1-dimentional picture of enhanced vertical mixing, one must invoke a full 3-D explanation: While the direct wind response brings nutrients to the surface inside the diffuse ice-edge, enhanced there by the increased mixing

energy, the resulting secondary mesoscale features are responsible for transports across the MIZ, for utilization by phytoplankton in the open water. One could then speculate that the view of the MIZ as a "hot spot" of biological productivity can be explained by its particular way of injecting energy available for mixing into the ocean and an enhancement of mixing in the *horizontal* plane. Thus, the cross-edge nutrient gradient becomes a governing quantity. Other authors ([Eilertsen and Wyatt, 2000]; [Falk-Petersen *et al.*, 2000]) have also found contrary evidence for the classical melt-water and growth hypothesis.

This important result not only applies to the MIZ: in the open ocean mesoscale variability emerges from unstable features caused by winds working on pre-existing current shears, inducing Ekman divergences [Smith *et al.*, 1996]. Another similarity is the apparent higher horizontal variability of the ecosystem fields than of the dynamical quantities.

A natural question is whether the conveying of nutrients into open water really has any significance when the ice-edge is retreating anyway during spring. Obviously it can serve as an initiation mechanism for secondary blooms, after the mixed layer has become void of nutrient in early spring. The eddy transport can also prolong the bloom season when the ice retreat is halting. Let's assume the Barents Sea ice edge is retreating 500 km over a 120 day growth season, with a 10 km band of 10 mmolN $m^{-2}d^{-1}$enhanced production, 0 elsewhere. If eddies can sustain a similar situation at the end of the season for further 10 days, then this contribution makes about 10% of the total production.

The net result in terms of production is of course dependent on the delicate combination of light and nutrient supply. In an area as the Fram Strait it could be of comparatively high importance compared to the shelf areas, due to the smaller seasonal amplitude of the ice extent.

The next question is whether the wind effect on creating eddies is at all important relative to other mechanisms such as baroclinic and barotropic instability of fronts, topography (in the Barents Sea), etc. Only a systematic investigation of different ocean states both by modelling and – not least – by new dedicated field experiments can provide the answer. From our model results we found that growth were enhanced inside cyclones shed from an up-welling structure. A frontal instability would tend to compress and shoal a water parcel turning into an anticyclone with biological growth [Spall and Richards, 2000]. So the observation of which kind of eddies have the most biological activity may hint at their generation mechanism. The present and related studies [Spall and Richards, 2000] show, however, that a bloom associated with a mesoscale feature is very transient by nature.

Viewed from the perspective of global warming the ocean biota may absorb a significant amount of anthropogenic carbon [Sarmiento and Le Quéré, 1996]. In an early compilation for the Arctic shelves [Walsh, 1989] suggested negative feedback from the biological system to greenhouse induced warming, since a larger area for primary production is opened during warming, implying net increased carbon fixation. [Johannessen and Miles, 2000] estimated this effect to 0.3–0.6 Pg C per year, or 15–30% of the present oceanic uptake. Currently, on a global basis, the counteracting effect of reduced uptake by the solubility pump due to a collapsed THC seems to dominate [Sarmiento and Le Quéré, 1996], even if there are large

remaining uncertainties conserning delayed structural responses of the ecosystems (due to acidity, extinctions etc.). Perhaps most important are the implications for the mixing regimes: If the character of the wind forcing is as important as may be claimed from our results, then one also need to consider the effect of large scale changes on the high frequency components of the atmosphere-ocean system in different geographical regions.

Considering the details of the forcing mechanisms, the ITL case is somewhat unrealistic in the sense that the wind event is long (4 days) compared with a typical low-presure passing (< 1 day), and that the stress gradient may be exaggerated due to the unrealistically stable iceward ABL. Nevertheless, the self-amplifying mechanism of momentum transfer to the ocean by the diverging ice, and the growth of pre-existing along-edge disturbances are well-known features of ocean response ([Häkkinen, 1987a]; [Niebauer and Smith, 1989]; Spall, 1996; [Smith *et al.*, 1996]). Indeed, our results are very similar to those of [Häkkinen, 1987a], except for the initiation of variability prior to wind on-set: Where we imposed variability in the MIZ system, [Häkkinen, 1987a] employed interaction of a barotropic current and a topographic structure. In both cases the ITL winds are seen to emphasize the pre-existing anomalies due to enhancement of stress gradients, while the opposite wind has a damping effect by pushing the ice iceward.

The most detailed relevant (empirical as well as numerical) study of vortex pairs and ice-tongues was that of [Johannessen *et al.*, 1994] in the EGC. Unsurprisingly, in this study the case of ITL was not observed, and the wind was ascribed a secondary role. In one case onset of ITR winds were said to destroy mesoscale variability, while in another case on-ice winds were suggested to be irrelevant to the development of ice-edge features. The latter case is puzzling in the view of our results: Ice tongues – evident in the observations – should be agents for imposing stress gradients on the ocean surface, with an immediate ocean response. So either the process of momentum transfer to the ice/ocean is much more complex than we assume, or the described wind event was short-lived (< 1 day). The damping effect of ITR winds, though, is in agreement with our findings: Ice features are compacted towards the main ice pack, and momentum transfer is hindered, although the fate of subsurface structures are not completely known, due to the inaccesibility regarding remote sensing. The indication of ice tongue generation in our study area supports the mechanism described above, but there are strong background currents influenced by topography as well as tides which complicates an interpretaiton.

The modelling of surface stress can also be decisive for eddy characteristics. With a wider initial MIZ than in the reference experiment, the upwelling region would be wider, accordingly, and hence cyclonic eddies may become larger. With expansion of the MIZ, as in the ITL case, eddies become stronger and the cross-edge tansport of nutrients and biomass is seen to bee more pronounced than in the opposite case. It is not the rotational direction of eddies that is decisive for cross-edge exchange, but their decay time and rotational speed which depend on the formation history.

Accordingly, their generation mechanism is essentially irrelevant; hence, other mechanisms such as baroclinic (and barotropic) instability of a pre-existing jet are possible. The case with

a turning wind showed indeed that an otherwise ITR dominated situation could be enhanced, subject to an intermittent ITL period, but preserving its qualitative behaviour.

Interaction of currents with topography ([Häkkinen, 1987b]; [Moseidjord *et al.*, 1999]) is also important, as mentioned above. Our results show unequivocally, however, that independent of generation mechanisms, a MIZ system has its inherent way of modifying a pre-existing mesoscale variability, depending on wind direction. Further modelling is needed, however, to investigate the robustness of the mechanism when a more realistic wind-stress formulation is employed, besides the effect of a pre-existing front/jet, topography, strength and wavelength of pre-existing disturbancies.

To conclude, we stress the need for better ice models and description of momentum transfer when operating at such small scales as we have done in the present study. However, we have demonstrated the validity of our simple process model of air-sea-ice-ecosystem interactions which can be modified to explore further aspects of MIZ dynamics.

Second, it is rather the eddy dynamics that has the major impact on the ecosystem. By providing mixing energy "horizontally", blooms can be sustained several days after the initiating wind event, and function as a horizontal analog of the deep chlorophyll maximum. The small scales involved (<10 km) brings into question the sampling strategies which usually assumes a much coarser resolution.

Appendix: 2-dimensional response experiments

In order to differentiate between the effects arising from along-edge variability from others, we investigate the pure cross-edge response for various stress profiles (Table).

Table 4. Description of 2-D experiments.

2d1	ABL	ice to the right
2d2	$\tau_{ice} = 2 \times \tau_{water}$	./.
2d3	$\tau_{ice} = 5 \times \tau_{water}$	./.
2dl1	ABL	ice to the left
2dl2	$\tau_{ice} = 2 \times \tau_{water}$	./.

First, the case with ice to the right is considered. In Fig. 24 one can see that in the simplest case, i.e. with the stress profile described as a step-function (Case 2d3), there is a single upwelling structure practically at the ice edge, i.e. at the step where there is maximum divergence of Ekman flow. This agrees well with the theory, and the signal decays to zero within about 10 km symmetrically to each side, i.e. a length scale comparable to R_d.

For the more realistic stress step (Case 2d2), shown for a 3 days wind episode, the response is qualitatively similar, although there are some wriggles on the MLD on the iceward side, due to the MLD becoming equal to the minimum allowable depth (set to 5 m). This minor deficiency of the model can easily be alleviated; in practice when using the ABL-parameterized stresses, the case never ocurred.

With the full ABL (Case 2d1) the dominant feature is a stress maximum approximately at intermediate ice concentrations, due to the combination of high roughness in the MIZ and intermediate turbulence level in the ABL. Hence, there is up-welling near the ice-edge (Ekman divergence) and down-welling under the ice (Ekman convergence); the characteristic antisymmetric pattern, in contrast to the step-cases. The up-welling signal is comparatively small because in the 10 km zone outside ice-edge the stress decays ice-ward with the specified ABL-thickness. Thus there is a weak over-all bias of the Ekman transport towards convergence, which can account for the weak asymmetry towards down-welling.

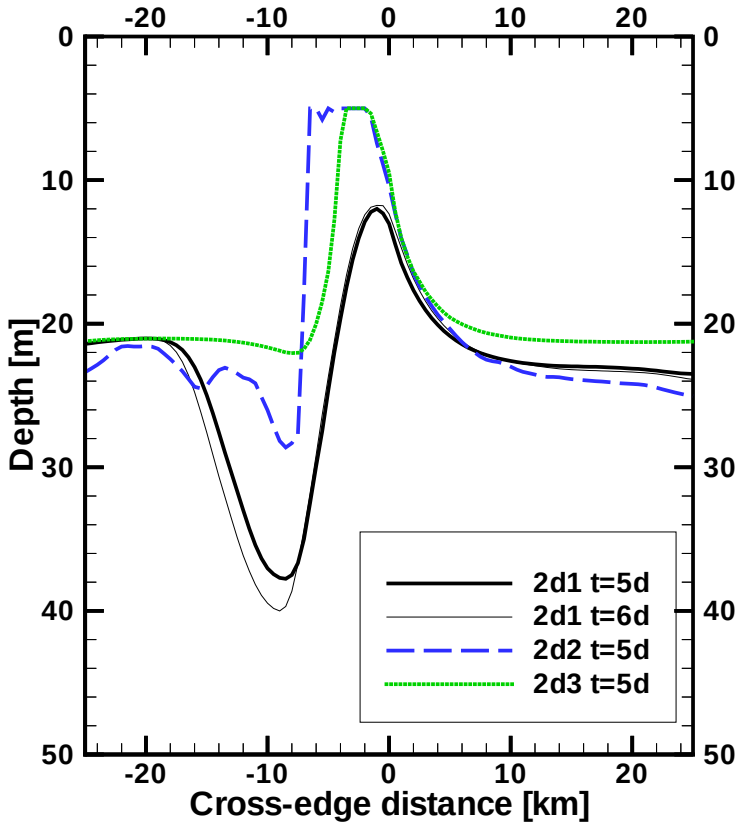

Figure 24. Depth of the ML after 1–3 days of wind forcing for the ice-to-the-right cases. 25 km has been cut at each side of the domain, in order to mask the irrelevant boundary currents

For th ITL case, Fig. 25 we first note that the full ABL case (2dl1) the response is not simply a mirror image of the corresponding ITR case. The downwelling region is shifted more off-edge (i.e. towards positive distance), due to the expanding ice cover. In addition, the upwelling region inside the ice-covered portion is indeed shoaling more intensely thant he ITR case, due to the comparatively stronger stress, due to the expansion of the stress maximum region.

For comparison a case with a single step in the stress at the ice edge is shown (case 2dl2), again showing a single downwelling structure, as expected. The somewhat broader structure relative to the ITR counterparts is probably due to the advancing ice edge. The slight wriggles

are caused by the inner MIZ opening up, as we used a criterion on ice concentration rather than the ice edge location to define the stress step.

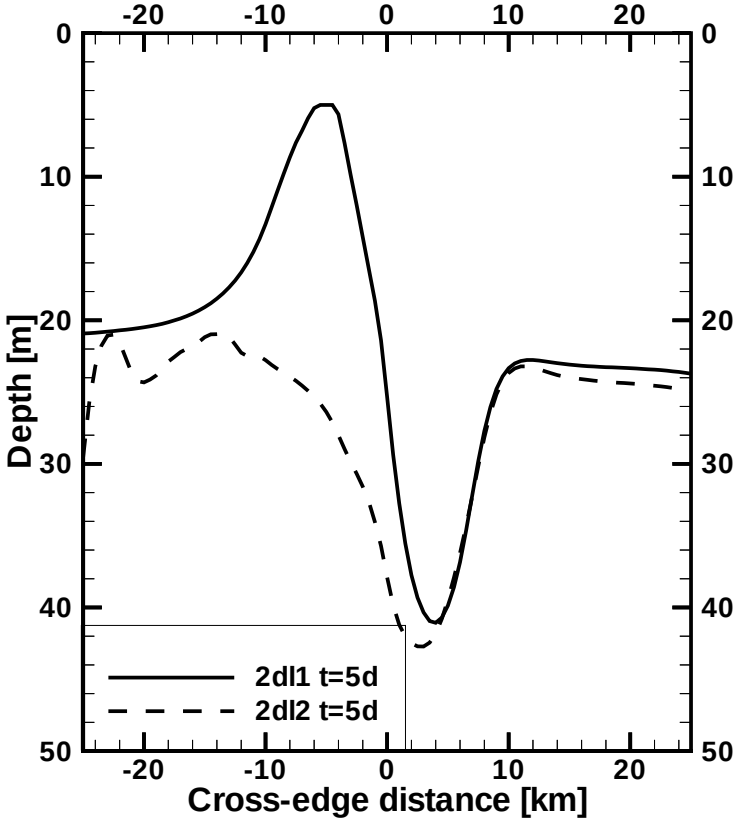

Figure 25. Depth of the ML after 2 days of wind forcing for the ice-to-the-left cases . 25 km has been cut at each side of the domain.

f

Acknowledgments. This project is funded by NFR. University of Bergen contributed with R/V *Håkon Mosby*. We thank the captain, crew and scientific staff onboard R/V *Håkon Mosby* for splendid co-operation. .
This is contribution no. 111117 from *G. C. Rieber Climate Institute* at NERSC

References

Backhaus, J. O., H. Wehde, E. Nøst Hegseth, and J. Kämpf, Phyto-Convection: On the Role of Oceanic Convection in Primary Production, *Mar. Ecol. Prog. Ser.*, pp. 77–92, 1999.

Båmstedt, U., H. C. Eilertsen, K. S. Tande, D. Slagstad, and H. R. Skjoldal, Copepod grazing and its potential impact on the phytoplankton development in the Barents Sea, *Polar Research*, *10*(2), 339–353, 1991.

Broström, G., *Interaction between mixed layer dynamics, gas exchange and biological production in the ocean surface layer with application to the northern North Atlantic*, Ph.D. thesis, Department of Oceanography, Göteborg University, 1997.

Broström, G., and H. Drange, On the mathematical formulation and parameter estimation of the Norwegian Sea plankton system, *Sarsia*, *85*, 211–225, 2000.

Buckley, J. R., T. Gammelsrød, J. A. Johannessen, O. M. Johannessen, and L. P. Røed, Upwelling: Oceanic structure at the edge of the Arctic ice pack in winter, *Science*, *203*, 165–167, 1979.

Drange, H., A 3-dimensional isopycnic coordinate model of the seasonal cycling of carbon and nitrogen in the Atlantic Ocean, *Phys. and Chem. of the Earth*, *21*, 503–509, 1997.

Drange, H., and K. Simonsen, Formulation of air-sea fluxes in the ESOP2 version of MICOM, *Tech. Rep.* 125, Nansen Environmantal and Remote Sensing Center, Bergen, Norway, 1997.

Eilertsen, H. C., J. P. Taasen, and J. M. Weslawski, Phytoplankton studies in the fjords of West Spitzbergen: physical environment and production in spring and summer, *J. Plankt. Res.*, *11*(6), 1245–1260, 1989.

Eilertsen, H. C., and T. Wyatt, Phytoplankton models and life history strategies, *S. Afr. J. Marine Sci.*, *22*, 323–338, 2000.

Fahrbach, E., J. Meincke, S. Osterhus, G. Rohardt, U. Schauer, V. Tverberg, and J. Verduin, Direct measurements of volume transports through Fram Strait, *Polar Research*, *20*, 214–221, 2001.

Falk-Petersen, S., H. Hop, W. P. Budgell, E. N. Hegseth, R. Korsnes, T. B. Loyning, J. B. Orbaek, T. Kawamura, and K. Shirasawa, Physical and ecological processes in the marginal ice zone of the northern Barents Sea during the summer melt period, *J. Mar. Syst.*, *27*, 131–159, 2000.

Fennel, W., and O. M. Johannessen, Wind forced oceanic responses near ice edges revisited, *J. Mar. Syst.*, *9*, 57–79, 1998.

Furevik, B. R., and O. M. J. nd A. D. Sandvik, SAR-retrieved wind in Polar Regions - Comparison with *in situ* data and atmospheric model output, *IEEE Trans. Geoscience and Rem. Sens.*, in press, 2002.

Guest, P. S., J. W. Glendening, and K. L. Davidsson, An observational and numerical study of wind stress variations within marginal ice zones, *J. Geophys. Res.*, *100*(C6), 10887–10904, 1995.

Häkkinen, S., Coupled ice-ocean dynamics in the marginal ice zones: upwelling/downwelling and eddy generation, *J. Geophys. Res.*, *91*(C1), 819–832, 1986.

Häkkinen, S., Feedback between ice flow, barotropic flow, and baroclinic flow in presence of bottom topogaphy, *J. Geophys. Res.*, *92*(C4), 3807–3820, 1987a.

Häkkinen, S., Upwelling at the ice edge: A mechanism for deep water formation?, *J. Geophys. Res.*, *92*, 5031–5034, 1987b.

Hibler, W. D., A dynamic thermodynamic sea-ice model, *J. Phys. Oceanogr.*, *9*, 815–846, 1979.

Ikeda, M., A coupled ice-ocean mixed layer model of the marginal ice zone responding to wnd forcing, *J. Geophys. Res.*, *94*(C7), 9699–9709, 1989.

Johannessen, J. A., O. M. Johannessen, E. Svendsen, R. Shuchman, T. Manley, W. J. Campbell, E. G. Josberger, S. Sandven, J. C. Gascard, T. Olaussen, K. Davidson, and J. VanLeer, Mesoscale eddies in the Fram Strait marginal ice zone durng the 1983 and 1984 Marginal Ice Zone Experiments, *J. Geophys. Res.*, *92*(C7), 6754–6772, 1987.

Johannessen, O. M., J. A. Johannessen, , J. Morison, B. Farrelly, and E. Svendsen, Oceanographic conditions in the marginal ice zone north of Svalbard in early fall 1979 with an emphasis on mesoscale processes, *J. Geophys. Res.*, *88*, 2755–2769, 1983.

Johannessen, O. M., and M. Miles, Arctic sea ice and climate chang — will the ice disappear in this century?, *Science Progress*, *83*, 209–222, 2000.

Johannessen, O. M., S. Sandven, W. P. Budgell, J. A. Johannessen, and R. A. Shuchman, Observation and simulation of ice tongues and vortex pairs in the marginal ice zone, in *Nansen Centennial Volume: The role of the Polar oceans in shaping the global climate*, edited by Johannessen, O. M., R. Muench, and J. Overland, pp. 95–108, American Geophysical Union Monograph, 1994.

Josberger, E., BOTTOM ABLATION AND HEAT-TRANSFER COEFFICIENTS FROM THE 1983 MARGINAL ICE-ZONE EXPERIMENTS , *J. Geophys. Res.*, *92*(C7), 7012–7016, 1987.

Kämpf, J., and J. O. Backhaus, Shallow, brine-driven free convection in polar oceans: Nonhydrostatic numerical process studies, *J. Geophys. Res.*, *103*(C3), 5577–5593, 1998.

Kimura, S., A. Kasai, H. Nakata, T. Sugimoto, J. H. Simpson, and J. V. S. Cheok, Biological productivity of meso-scale eddies casused by frontal disturbances in the Kuroshio, *ICES Journal of Marine Science*, *54*, 179–192, 1997.

Kuzmina, N. P., On the parameterization of interleaving and turbulent mixing using CTD data from the Azores Frontal Zone, *J. Mar. Syst.*, *23*, 285–302, 2000.

Mahadevan, A., and D. Archer, Modeling the impact of fronts and mesoscale circulation on the nutrient supply and biogeochemistry of the upper ocean, *J. Geophys. Res.*, *105*(C1), 1209–1225, 2000.

Manley, T. O., and W. O. Smith, Transport of biogenic particulate matter to depth within the Greenland Sea, in *Nansen Centennial Volume: The role of the Polar oceans in shaping the global climate*, edited by Johannessen, O. M., R. Muench, and J. Overland, pp. 223–236, American Geophysical Union Monograph, 1994.

Martin, A. P., K. J. Richards, and M. J. R. Fasham, Phytoplankton production and community structure in an unstable frontal region, *J. Mar. Syst.*, *28*, 65–89, 2001.

May, B. D., and D. E. Kelley, Effect of baroclinicity on double-diffusive interleaving, *J. Phys. Oceanogr.*, *25*, 1997–2008, 1997.

McGillicuddy, D., R. Johnson, D. Siegel, A. Michaels, N. Bates, and A. Knap, Mesoscale variations of biogeochemical properties in the Sargasso Sea, *J. Geophys. Res.*, *104*(C6), 13381–13394, 1999.

Moseidjord, H., H. Svendsen, and D. Slagstad, Sensitivity studies of circulation and ocean-shelf exchange off northern Norway, *Sarsia*, *84*, 191–198, 1999.

Niebauer, H. J., and W. O. J. Smith, A numerical model of mesoscale physical-biological interactions in the Fram Strait marginal ice zone, *J. Geophys. Res.*, *94*(C11), 16151–16175, 1989.

Pomeroy, L. A., Primary production in the Arctic Ocean estimated from dissolved oxygen, *J. Mar. Syst.*, *10*, 1–8, 1997.

Sakshaug, E., A. Bjørge, B. Gulliksen, H. Loeng, and F. Mehlum, *Økosysem Barentshavet*, pp. 91–108, Norges Allmennvitenskpelige Forskningsråd, Norges Fiskeriforskningsråd, Miljøverndepartementet, 1992.

Sandven, S., and O. M. Johannessen, The use of microwave remote-sensing for sea ice studies in the Barents Sea, *ISPRS JOURNAL OF PHOTOGRAMMETRY AND REMOTE SENSING*, *48*, 2–18, 1993.

Sandven, S., O. M. Johannessen, and J. A. Johannessen, Mesoscale eddies and chimneys in the marginal ice zone, *J. Mar. Syst.*, *2*, 195–208, 1991.

Sarmiento, J., and C. Le Quéré, Oceanic carbon dioxide uptake in a model of century-scale global warming, *Science*, *274*, 1346–1350, 1996.

Smith, C. L., K. J. Richards, and M. J. R. Fasham, The impact of mesoscale eddies on plankton dynamics in the upper ocean, *Deep-Sea Res.*, *43*(11-12), 1807–1832, 1996.

Smith, W. O., Phytoplanktondynamics in marginal ice zones, *Oceanogr. Mar. Biol. Ann. Rev*, *25*, 11–38, 1987.

Spall, S. A., and K. J. Richards, A numerical model of mesoscale frontal variabilities and plankton dynamics — I. Model formulation and initial experiments, *Deep-Sea Res.*, *47*, 1261–1301, 2000.

Uz, B. M., J. A. Yoder, and V. Osychny, Pumping of nutrients to ocean surface waters by the action of propagating planetary waves, *Nature*, *406*, 597–600, 2001.

Walsh, J. J., Arctic carbon sinks: present and future, *Glob. Biog. Cyc.*, *3*, 393–411, 1989.

K. Lygre, Nansen Environmental and Remote Sensing Center, Edvard Griegsvei 3a, N–5059 Bergen, Norway. (e-mail: kjetil.lygre@nrsc.no)

Received ; revised ; accepted .